LUND UNIVERSITY

A scattering study of concentrated lens protein solutions and mixtures - Towards understanding the molecular origin of presbyopia

Bucciarelli, Saskia

2015

A scattering study of concentrated lens protein solutions and mixtures

Towards understanding the molecular origin of presbyopia

PHYSICAL CHEMISTRY | FACULTY OF SCIENCE | LUND UNIVERSITY
SASKIA BUCCIARELLI

A scattering study of concentrated lens protein solutions and mixtures

Towards understanding the molecular origin of presbyopia

Saskia Bucciarelli

Organization: LUND UNIVERSITY Physical Chemistry Division P.O. Box 124 221 00 Lund, Sweden	Document name: DOCTORAL DISSERTATION
	Date of issue: 2015-12-11
Author: Saskia Bucciarelli	Sponsoring organization:

Title and subtitle:
A scattering study of concentrated lens protein solutions and mixtures - Towards understanding the molecular origin of presbyopia

Abstract:

Healthy eye lenses are transparent and flexible, able to adapt shape in order to focus on far away and close-by objects. With age, however, this flexibility is lost, leading to a condition known as presbyopia. This vision disorder where close-by objects appear blurred commonly starts around the age of 40. The aim of this thesis is to elucidate the molecular origin of the gradual hardening of the core of the eye lens, made of fibre cells filled with concentrated mixtures of proteins, the so-called crystallins, which leads to the formation of presbyopia. To this end, various scattering techniques, static and dynamic light scattering (SLS & DLS), small-angle X-ray scattering (SAXS) and neutron spin echo (NSE), are used to study solutions of crystallins at concentrations up to those present in the lens.

The first part of this work deals with solutions of the individual proteins. We show that different techniques allow us to access solution dynamics on different length scales. While DLS probes the collective dynamics, NSE accesses length scales corresponding to the average distance between nearest neighbors in the solution. We find that the dynamic behavior of protein solutions depends on the nature of the protein interactions, as well as on their patchiness. For the largest of the lens proteins, α-crystallin, well described by a model of polydisperse (20%) colloidal hard spheres, we find a slowing down of the local dynamics over a large range of volume fractions ϕ and macroscopic arrest due to caging by neighboring particles at $\phi \approx 58\%$. The highly polydisperse βH-crystallin, in addition to hard sphere repulsion, exhibits a weak short-range attraction of the order of $0.5 k_B T$. At intermediate to high ϕ, the attractions lead to slower local dynamics compared to the pure hard sphere case, but the polydispersity pushes macroscopic arrest to $\phi \approx 62\%$. The smallest of the lens proteins, γB-crystallin, is known to exhibit short-range attractions of the order of about $1 k_B T$ which lead to phenomena such as liquid-liquid phase separation and spinodal decomposition. We now showed that γB-crystallin undergoes macroscopic arrest at $\phi \approx 35\%$ where caging effects are still negligible. Moreover, on collective length scales we find a competition between critical slowing down, related to the existence of a critical point at $\phi \approx 15\%$, and dynamical arrest at larger volume fractions. NSE allows us to disentangle these effects and study the short-time local dynamics of the protein solutions. Combining these results with computer simulations, we are able to show that an enormous slowing down such as the one observed for γB-crystallin can only be explained by patchy attractions which lead to the formation of transient space-spanning clusters.

The second part of this thesis is dedicated to the study of the solution dynamics of binary $\alpha/\gamma B$ or $\beta H/\gamma B$ mixtures. We find that these mixtures are also subject to critical concentration fluctuations and that they are strongly slowed down with increasing ϕ, enhanced by mutual α-γB and βH-γB interactions.

Key words:
scattering, dynamics, arrest, eye lens, proteins, crystallins, concentrated, crowding, presbyopia, SAXS, SLS, DLS, NSE

Classification system and/or index terms (if any):

Supplementary bibliographical information:	Language: English
ISSN and key title:	ISBN: 978-91-7422-419-1

Recipient´s notes:	Number of pages: 200	Price:
	Security classification:	

Signature: _Bucciarelli_   Date: 02.11.2015

A scattering study of concentrated lens protein solutions and mixtures

Towards understanding the molecular origin of presbyopia

Saskia Bucciarelli

LUND UNIVERSITY

Contents

detector

scattering pattern

scattered beam

θ

sample

sample-detector distance L

rp images of the
ves, others have
ks or documents
and eventually
as **presbyopia**,
? To be able to
he eye is build.
in components.
eye through the

pupil

lens

retina

iris

cornea

Figure 1: Simplified schematic of an eye. The cornea is the transparent layer covering the front of the eye. The iris acts as a diaphragm, controlling the size of the pupil which is the adjustable aperture through which light enters the eye. The eye color is due to the color of the iris. The ocular lens, together with the cornea is in charge of focusing the light entering through the pupil onto the retina, a light-sensitive tissue that transmits light impulses to the nerve cells that transport them to the brain.

retina

lens

retina

focal point

focal point

pupil, no matter how far away its source, has to be focused onto the retina where the image is formed. If the focal point is shifted away from the retina, the image appears blurred. From optics, it is known that the focal point of a simple lens depends on its curvature and on the distance between the light source and the lens. For an unflexible, rigid lens with fixed curvature, light emitted by close objects thus has a different focal point than light coming from far away objects. For the eye, this means that the lens has to adjust shape to be able to focus light

primary beam

scattered beam

sample

θ

sample-detector distance L

pupil

lens

retina

cornea

iris

lens

retina

focal point

lens
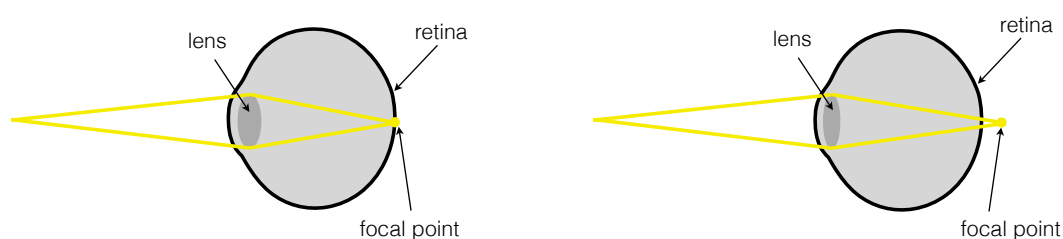
retina

focal point

Figure 2: Schematic of the focusing of light of a healthy eye (left) where the focal point is located on the retina and of an eye with presbyopia (right) where the focal point is shifted behind the retina.

The lens is formed of fibre cells that are filled with very concentrated solutions of proteins, known as crystallins that can be divided into three major classes: α-, β- and γ-crystallins. The sizes of these proteins range from 3.6 nm (γ-crystallin) to 16 nm (α-crystallin), where 1 nm = 0.000000001 m (a strand of human hair has a diameter of about 180 000 nm). So-called *scattering techniques* are ideally suited to study particles as small as the crystallins. They are based on irradiating a sample (with either laser light, X-rays or neutrons) and analyzing the radiation that is scattered by the sample. I used a variety of different scattering techniques, allowing me to analyze the interactions, stability and diffusion (movement) of crystallins in solution.

Proteins are rather complex structures, but to analyze the results obtained from scattering experiments, they can be simplified (see figure 3) and described as either *hard spheres* (comparable to tiny billiard balls that do not interact with each other, except for the fact that they cannot occupy the same space at the same time) or *short-range attractive hard spheres* (comparable to tiny billiard balls that attract each other/stick together when they come close, but do not feel each other at larger separations). This approach was applied to solutions of crystallins at varying concentration, from very dilute to very concentrated. These proteins were purified from calf eye lenses purchased as a by-product from a
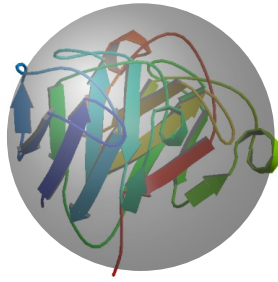
Figure 3: Protein structure and the sphere used to model the protein (in gray).

local slaughterhouse. In a first step, only solutions of the individual proteins were studied and the main focus was put on their dynamic behavior. It was found that at concentrations comparable to those found in the eye lens, these solutions undergo a so-called *dynamical arrest*, leaving the solution in a glassy or gel-like, rather than fluid, state. In an attempt to further mimic conditions found in the eye, binary mixtures of different proteins were studied and while this study is far from complete, it does point in the same direction as the trend found for individual protein solutions, namely a dynamical arrest at physiologically relevant concentrations. While a lens filled with a fluid-like concentrated protein solution is able to adapt its shape to adjust focus, a lens with a dynamically arrested mixture of proteins becomes stiff and can no longer accommodate for close vision. The study presented here thus provides very compelling evidence for the hypothesis that age-related dynamical slowing down and eventual arrest of the concentrated protein mixture in the eye lens fibre cells leads to the gradual hardening of the eye lens that is at the origin of presbyopia.

List of Papers

I. Hard sphere-like glass transition in eye lens α-crystallin solutions
   G. Foffi, G. Savin, S. Bucciarelli, N. Dorsaz, G. M. Thurston, A. Stradner
   and P. Schurtenberger
   Proc. Natl. Acad. Sci. U.S.A., **2014**, *111*, 16748–16753

II. Dramatic slowing down of short-time diffusion in crowded protein solutions
    – insight from neutron spin echo measurements
    S. Bucciarelli, J.-S. Myung, B. Farago, S. Das, G. Vliegenthart, O. Holderer,
    R. G. Winkler, P. Schurtenberger, G. Gompper and A. Stradner
    manuscript

III. Arrest scenarios in lens protein solutions – a colloid approach to presbyopia
     S. Bucciarelli, L. Casal-Dujat, C. Jud, M. Jéhannin, O. Holderer, G. M.
     Thurston, B. Farago, P. Schurtenberger and A. Stradner
     manuscript

IV. Eye lens βH-crystallin: to be or not to be hard spheres
    S. Bucciarelli, N. Skar-Gislinge, L. Casal-Dujat, T. Garting, N. Mahmoudi,
    M. Obiols-Rabasa, B. Farago, P. Schurtenberger and A. Stradner
    manuscript

V. Unusual dynamics of concentration fluctuations in solutions of weakly
   attractive globular proteins
   S. Bucciarelli, L. Casal-Dujat, C. De Michele, F. Sciortino, J. Dhont, J.
   Bergenholtz, B. Farago, P. Schurtenberger and A. Stradner
   J. Phys. Chem. Lett., **2015**, *6*, 4470–4474

List of Contributions

I. I performed the DLS measurement of the most concentrated sample and contributed to the final editing and proof-reading of the manuscript.

II. I performed all the experimental work with help from the co-authors (for the NSE experiments), did all the data treatment and wrote the manuscript together with the co-authors.

III. I performed all the experimental work in collaboration with L. Casal-Dujat and M. Jéhannin with help from the co-authors (for the NSE experiments), did all the data treatment and wrote the manuscript together with the co-authors.

IV. I contributed to the experimental work, did all the data treatment (except for the viscosity experiments) and wrote the manuscript with input from the co-authors.

V. I performed all the experimental work in collaboration with L. Casal-Dujat with help from the co-authors (for the NSE experiments), did all the data treatment and wrote the manuscript together with the co-authors.

VI. I performed all the experimental work in collaboration with L. Casal-Dujat with help from the co-authors (for the NSE experiments), did all the data treatment and wrote the manuscript with input from the co-authors.

VII. I contributed to the experimental work, did most of the data treatment and wrote the manuscript together with N. Mahmoudi with input from the co-authors.

Papers Not Included in the Thesis

I. Cluster-driven dynamical arrest in concentrated lysozyme solutions
    F. Cardinaux, E. Zaccarelli, A. Stradner, S. Bucciarelli, B. Farago, S. U.
    Egelhaaf, F. Sciortino, P. Schurtenberger
    J. Phys. Chem. B, **2011**, *115*, 7227–7237

Acknowledgements

▷ To my supervisors Anna Stradner and Peter Schurtenberger: Thank you for convincing me to come to Sweden and for giving me the opportunity to work on this very interesting project. I learned a lot over the last years!

▷ A huge Thank You! to my colleagues and office mates, Najet, Nicholas and Tommy for many nice discussions and for all your support. You helped me so much, especially during the last months of my PhD, and I am indefinitely grateful to you. To all my office mates over the years: It was a real pleasure to share office with you!

▷ I also have to thank Corinne and Yuki who prepared me so well for this project. It was great to work with you and this thesis would not have been possible without you!

▷ Marc, thank you so much for all your help with instruments, experiments and much more!

▷ I also want to thank the local contacts at the large scale facilities, Bela Farago at the Institut Laue-Langevin (ILL) in Grenoble, France and Olaf Holderer at the Heinz Maier-Leibnitz Zentrum (MLZ) in Garching, Germany, for the help with the NSE measurements.

▷ Coco Michel et tout le personnel à Marmy SA: merci pour la bonne coopération!

▷ I want to thank George Thurston for very intense and interesting discussions.

▷ Christopher, Maria S., Ingrid and Helena: You were always so helpful with administrative and technical errands, thank you very much for that! I also want to thank Ingegerd and Lennart for the help with setting up everything after the move to Sweden.

▷ To all the people at Physical Chemistry in Lund: Thank you for creating such a great working environment!

▷ To Lina and the people at LL Dance Studio: Thank you for being so warm and welcoming. You made settling in Sweden much easier and provided me with a wonderful balance to work. Keep up the good work, you guys are fabulous!

▷ To Emelie, Solmaz, Jessie, Divya and Johanna: thank you so much for your friendship and support throughout the years, for many nice girls' days, brunches, lunches, linners and dinners. You really made the last 4.5 years worthwhile and I can't imagine not seeing you this often anymore. I hope that we will stay in touch, no matter where we will all end up! Melissa, thank you for your continuous friendship and for taking care of my mental health ;-) I love you!

▷ Till 'The Malkkis': Tack för att ni välkomnade mig i er familj! Jag är så glad över att vara en del av det!

▷ Mama, Papa, villmools Merci, dass där emmer u mech gegleewt hutt a mech emmer ennerstëtzt, egal waat ech mer an de Kapp setzen. Ouni äerch wäer ech net do, wou ech elo sin an äere Réckhalt bedeit mer onendlech vill. Sandro an Thiemo: et ass schéin, äerch a mengem Liewen ze hun, och wa mer kee besonneg regelméissege Kontakt hun!

▷ And finally, my wonderful husband, Erkki. Thank you so much for your constant interest in my work, for proofreading my popular science summary, for your love, patience and support. You make everything so much easier. I love you more than words can say!

List of Symbols

N_A	Avogadro constant
B_2	second virial coefficient
c	protein concentration
D_0	free diffusion coefficient
D_c	collective diffusion coefficient
ΔR_θ	excess Rayleigh ratio
κ_T	osmotic compressibility
$D_s(q)$	short-time local diffusion coefficient
η	viscosity
$g_1(t)$	field autocorrelation function
$g_2(t)$	intensity autocorrelation function
Γ	decay constant
$I(q)$	scattering intensity
K	optical constant
k_B	Boltzmann constant
λ	wavelength of the radiation
M_w	molecular weight
n	refractive index
ϕ	volume fraction
ϕ_{arr}	arrest volume fraction
ϕ_{c}	critical volume fraction
ϕ_{eff}	effective volume fraction
ϕ_{tot}	total volume fraction
pI	isoelectric point
$P(q)$	particle form factor
q	magnitude of the scattering vector $\mathbf{q}$
d^*	average nearest-neighbor distance
q^*	q-value corresponding to d^*
R_g	radius of gyration

$R_{h,0}$	hydrodynamic radius of a non-interacting protein in solution
$R_{h,\text{app}}$	apparent hydrodynamic radius of interacting proteins in solution
σ	polydispersity
$S(q)$	static structure factor
T	temperature
T_c	critical temperature
θ	scattering angle
U_a	strength of attractive interaction potential
v	voluminosity
ξ_d	dynamic correlation length

List of Abbreviations

ACF   autocorrelation function
CS   Carnahan-Starling
DLS   dynamic light scattering
ELCS   extended law of corresponding states
HS   hard sphere
IEX   ion exchange chromatography
ISF   intermediate scattering function
LS   light scattering
MALS   multiangle light scattering
NSE   neutron spin echo
SAXS   small-angle X-ray scattering
SEC   size-exclusion chromatography
SLS   static light scattering

Part I

INTRODUCTION

1
The eye lens

1.1 Function and structure

An important part of the mammalian eye is the lens which is responsible for focusing incoming light onto the retina. In order to enable clear and sharp vision, the lens has to be highly optically transparent, have a large refractive index and be flexible. While a large refractive index and flexibility of the lens enable adaptive focusing of the light onto the retina, i.e. near and far vision, transparency prevents scattering of the incoming light, which would lead to a blurred image of the outside world. To fulfill all of these tasks, nature has created very elongated lens fibre cells (cf. figure 1.1) containing a highly concentrated mixture of proteins called crystallins, present at total concentrations of up to more than 500 mg/ml [1, 2], corresponding to total volume fractions ϕ_{tot} of about 50–60%. These exceptionally high concentrations are at the origin of the large refractive power of the eye lens. In order for the lens to remain flexible, it is crucial that the aqueous protein mixture inside the lens fibre cells is in a fluid-like state. To ensure transparency, the lens fibre cells are regularly ordered and tightly packed within the lens. To further avoid scattering of incoming light, the lens is devoid of blood vessels and the fibre cells lose all organelles as they move towards the nucleus of the lens during differentiation [5], as depicted in figure 1.1. The lack of organelles in mature eye lens fibre cells means that there is no protein
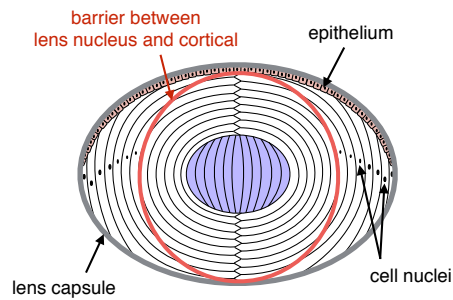
Figure 1.1: Schematic of a mammalian eye lens surrounded by a transparent membrane, the lens capsule. The anterior of the lens is covered in a single layer of epithelium. Located at the centre of the lens are the primary lens fibre cells (shown in purple) which have been differentiated from the posterior epithelial cells. This so-called embryonic lens nucleus is surrounded by the secondary lens fibers that have been differentiated from the equatorial epithelium. During differentiation, the eye lens fibre cells degrade their organelles, in order to assure lens transparency [3, 4].

turn-over in the cells, i.e. every protein in these cells has to last the lifetime of the individual [6]. Another crucial prerequisite for lens transparency is a homogeneous packing of the crystallins within the lens fibre cells, thus preventing microscopic spatial fluctuations of the refractive index of the protein mixture, as spatial inhomogeneities would lead to scattering of the incoming light, and, as a consequence, to blurred vision [7–9].

1.2 Disorders of the lens

A multitude of ocular diseases can impair proper vision, some of them being related to the eye lens. I will focus on the molecular origin of two of the most common of those medical conditions: cataract and presbyopia.

1.2.1 Cataract

In the aging lens, the concentrated protein mixture in the fibre cells can become unstable and form aggregates that scatter incoming light, thus turning the lens cloudy. As the disease progresses, the lens will eventually become fully turbid, causing a complete loss of eye sight [10, 11]. This clouding of the lens is known as cataract, a so-called protein condensation disease that, according to the World Health Organization (WHO), is one of the leading causes of visual impairment worldwide [12]. In an attempt to better understand the molecular origin of this condition affecting nearly 18 million people worldwide [13], an extensive study of the structural properties, phase behavior and stability of pure eye lens protein

solutions [10, 14, 15], as well as mixtures [16–19] has been started. The complex design of the lens with its varying protein content however makes a complete characterization rather challenging.

1.2.2 Presbyopia

The word presbyopia stems from the greek words *présbys* (old, old man) and *ops* (eye, face, sight) and describes a very common age-related vision disorder, usually starting around the age of 40. Young and healthy lenses are soft and flexible, allowing them to change shape to adapt focus in order to produce sharp close-up, as well as distant images. Upon aging, however, the nucleus of the lens becomes increasingly stiff, compromising accommodation to near targets by shifting the focal point behind the retina [11, 20–25]. While distant vision remains unaffected by this hardening of the core of the lens, focusing up close becomes more and more difficult. To this date, the molecular origin of this stiffening of the lens nucleus that is at the origin of presbyopia is not well known and is the main focus of the work presented in this thesis.

1.3 Crystallins

There are three major classes of lens crystallins in the mammalian eye: α-, β- and γ-crystallin. While the latter is most abundant in the nucleus of the lens, α- and β-crystallin are mostly found in the cortical [26]. Under physiological conditions, the aqueous protein solution in the eye lens cells has a pH of 6.8 and contains 17–150 mM KCl [27]. The study presented in this thesis focuses on crystallins of the species Bos taurus (cattle).

1.3.1 α-crystallin

Eye lens α-crystallins are polydisperse multimers made up of αA (molecular weight M_w = 19.9 kDa) and αB (M_w = 20.2 kDa) subunits [6, 27], shown in figure 1.2. They are non-compact proteins [28] with a molecular weight ranging from 300 to 1200 kDa, with an average of around 800 kDa [29]. Besides functioning as structural proteins, they also act as chaperones, binding β- and γ-crystallin at the onset of their denaturation, thus preventing non-specific aggregation and maintaining lens clarity [29, 32–35]. With an isoelectric point (pI) of around 4.5 [14], α-crystallin is highly negatively charged at physiological pH. However, at physiological ionic strength, electrostatic interactions are well
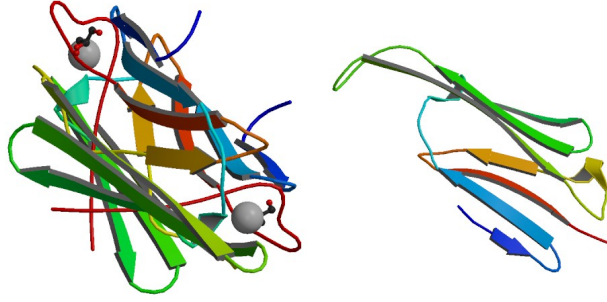
Figure 1.2: Biological assembly, i.e. the functional form of bovine αA (left) [30] and human αB (right) [31]. Alpha helices and beta strands are shown as ribbons with arrowheads pointing towards the carboxy (C) termini. The quaternary structure represented here is rainbow-colored from blue (N-terminal) to red (C-terminal).

screened [36] and hence this charge only matters in the vicinity of the protein surface, preventing them from aggregating [27].

1.3.2 β-crystallin

β-crystallins are highly polydisperse oligomeric proteins with a pI around 8, i.e. slightly positively charged at physiological pH. They can be separated into three size classes: βH (octamers, M_w = 160–200 kDa), βL_1 (trimers/tetramers, $M_w \approx 71$ kDa) and βL_2 (dimers, $M_w \approx 46$ kDa) [37, 38]. The family of mammalian β-crystallin comprises 7 members that aggregate to form these oligomers: $\beta A1$ (M_w = 23.2 kDa), $\beta A2$ (M_w = 22.0 kDa), $\beta A3$ (M_w = 25.2 kDa), $\beta A4$ (M_w = 22.2 kDa), $\beta B1$ (M_w = 27.9 kDa), $\beta B2$ (M_w = 23.2 kDa, figure 1.3) and $\beta B3$ (M_w = 24.2 kDa) [27, 39]. In this work, I focus on the high-M_w βH-crystallin.
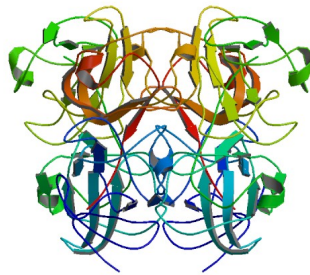
Figure 1.3: Biological assembly of bovine $\beta B2$ [40]. Alpha helices and beta strands are shown as ribbons with arrowheads pointing towards the C-termini. The quaternary structure represented here is rainbow-colored from blue (N-terminal) to red (C-terminal).

6

1.3.3 γ-crystallin

The smallest eye lens proteins are the monomeric compact γ-crystallins, a family of globular proteins comprising 6 members: γS, γA, γB, γC, γD and γE. They can be classified according to their critical temperature T_c into high-T_c and low-T_c proteins. I focus my studies on the low-T_c γB-crystallin [41] (figure 1.4) which has a molecular weight of 21.097 kDa [42] and a pI around 7, i.e. it is close to neutral at physiological pH. The interactions are then mainly due to short-range attractive van der Waals forces [27].

Figure 1.4: Biological assembly of bovine γ_B [43]. Alpha helices and beta strands are shown as ribbons with arrowheads pointing towards the C-termini. The quaternary structure represented here is rainbow-colored from blue (N-terminal) to red (C-terminal).

1.4 Protein-colloid analogy

It has been shown that applying concepts from colloid science to proteins by coarse-graining them, i.e. omitting their structural details and representing them as colloidal particles with an effective interaction potential, can be very fruitful in the quest to understand proteins in solution [44–47]. This approach has in fact already been applied to eye lens proteins to describe their interactions and structural properties. α-crystallin, for example, is well described by a model of (polydisperse) colloidal hard spheres [14, 36, 48]. For γB-crystallin, on the other hand, a model of short-range attractive hard spheres has traditionally been used [15, 17, 49, 50]. Surprisingly, up to now, to my knowledge, no full characterization of βH-crystallin is available. Tardieu et al. [51] have reported a rather limited study of β-crystallin interactions and concluded that they are repulsive, similar to α-crystallin, but more data is clearly necessary to verify this finding.

In this work, I will show that drawing an analogy between proteins and colloids does not only allow for an accurate description of the protein-protein interactions and their solution structure, but that it can, to a certain extend, also be applied to the dynamic properties of eye lens protein solutions.

1.5 Macromolecular crowding

As mentioned previously, the eye lens fibre cells are filled with highly concentrated protein mixtures, i.e. under physiological conditions every protein feels the presence of its nearest neighbors, even more so if these neighbors exhibit a short-range attractive interaction potential. In recent years, this effect exerted by the surrounding molecules, known as macromolecular crowding, has received increasing attention [52–55]. It has become clear that in order to understand protein dynamics in concentrated solutions, such as those present in the lens, it is crucial to take into account crowding effects. The study presented in this thesis therefore covers a large concentration range, up to values corresponding to those in the ocular lens.

References

(1)   Vérétout, F.; Tardieu, A. *Eur. Biophys. J.* **1989**, *17*, 61–68.
(2)   Zhao, H.; Magone, M. T.; Schuck, P. *Phys. Biol.* **2011**, *8*, 046004 (10pp).
(3)   Song, S.; Landsbury, A.; Dahm, R.; Liu, Y.; Zhang, Q.; Quinlan, R. A. *J. Clin. Invest.* **2009**, *119*, 1837–1848.
(4)   Dahm, R.; van Marle, J.; Quinlan, R. A.; Prescott, A. R.; Vrensen, G. F. J. M. *Phil. Trans. R. Soc. B* **2011**, *366*, 1265–1277.
(5)   Bassnett, S. *Exp. Eye Res.* **2002**, *74*, 1–6.
(6)   Wistow, G. J.; Piatigorsky, J. *Ann. Rev. Biochem.* **1988**, *57*, 479–504.
(7)   Benedek, G. B. *Appl. Opt.* **1971**, *10*, 459–473.
(8)   Delaye, M.; Tardieu, A. *Nature* **1983**, *302*, 415–417.
(9)   Tardieu, A.; Delaye, M. *Ann. Rev. Biophys. Biophys. Chem.* **1988**, *17*, 47–70.
(10)   Benedek, G. B. *Invest. Ophthalmol. Vis. Sci.* **1997**, *38*, 1911–1921.
(11)   Petrash, J. M. *Invest. Ophthalmol. Vis. Sci.* **2013**, *54*, ORSF54–ORSF59.
(12)   http://www.who.int/mediacentre/factsheets/fs282/en/.
(13)   Rao, G. N.; Khanna, R.; Payal, A. *Curr. Opin. Ophthalmol.* **2011**, *22*, 4–9.
(14)   Finet, S.; Tardieu, A. *J. Cryst. Growth* **2001**, *232*, 40–49.
(15)   Stradner, A.; Thurston, G. M.; Schurtenberger, P. *J. Phys.: Condens. Matter* **2005**, *17*, S2805–S2816.

(16) Stradner, A.; Thurston, G.; Lobaskin, V.; Schurtenberger, P. *Progr. Colloid Polym. Sci.* **2004**, *126*, 173–177.

(17) Stradner, A.; Foffi, G.; Dorsaz, N.; Thurston, G.; Schurtenberger, P. *Phys. Rev. Lett.* **2007**, *99*, 198103.

(18) Dorsaz, N.; Thurston, G. M.; Stradner, A.; Schurtenberger, P.; Foffi, G. *J. Phys. Chem. B* **2009**, *113*, 1693–1709.

(19) Dorsaz, N.; Thurston, G. M.; Stradner, A.; Schurtenberger, P.; Foffi, G. *Soft Matter* **2011**, *7*, 1763–1776.

(20) Glasser, A.; Campbell, M. C. W. *Vision Res.* **1999**, *39*, 1991–2015.

(21) Bron, A. J.; Vrensen, G. F. J. M.; Koretz, J.; Maraini, G.; Harding, J. J. *Ophthalmol.* **2000**, *214*, 86–104.

(22) Heys, K. R.; Cram, S. L.; Truscott, R. J. W. *Mol. Vis.* **2004**, *10*, 956–963.

(23) Weeber, H. A.; Eckert, G.; Soergel, F.; Meyer, C. H.; Pechhold, W.; van der Heijde, R. G. L. *Exp. Eye Res.* **2005**, *80*, 425–434.

(24) Weeber, H. A.; Eckert, G.; Pechhold, W.; van der Heijde, R. G. L. *Graef. Arch. Clin. Exp. Ophthalmol.* **2007**, *245*, 1357–1366.

(25) Weeber, H. A.; van der Heijde, R. G. L. *Exp. Eye Res.* **2007**, *85*, 602–607.

(26) Siezen, R. J.; Fisch, M. R.; Slingsby, C.; Benedek, G. B. *Proc. Natl. Acad. Sci. U.S.A.* **1985**, *82*, 1701–1705.

(27) Bloemendal, H.; de Jong, W.; Jaenicke, R.; Lubsen, N. H.; Slingsby, C.; Tardieu, A. *Prog. Biophys. Mol. Biol.* **2004**, *86*, 407–485.

(28) Vanhoudt, J.; Aerts, T.; Abgar, S.; Clauwaert, J. *Int. J. Biol. Macromol.* **1998**, *22*, 229–37.

(29) Horwitz, J. *Proc. Natl. Acad. Sci. U.S.A.* **1992**, *89*, 10449–10453.

(30) Laganowsky, A.; Benesch, J. L. P.; Landau, M.; Ding, L.; Sawaya, M. R.; Cascio, D.; Huang, Q.; Robinson, C. V.; Horwitz, J.; Eisenberg, D. *Prot. Sci.* **2010**, *19*, 1031–1043.
PDB ID: 3L1E

(31) Bagnéris, C.; Bateman, O. A.; Naylor, C. E.; Cronin, N.; Boelens, W. C.; Keep, N. H.; Slingsby, C. *J. Mol. Biol.* **2009**, *392*, 1242–1252.
PDB ID: 2WJ7

(32) Rao, P. V.; Huang, Q. L.; Horwitz, J.; Zigler, J. S. *Biochim. Biophys. Acta* **1995**, *1245*, 439–47.

(33) Horwitz, J.; Bova, M. P.; Ding, L.; Haley, D. A.; Stewart, P. L. *Eye* **1999**, *13*, 403–408.

(34) Derham, B. K.; Harding, J. J. *Progr. Ret. Eye Res.* **1999**, *18*, 463–509.

(35) Horwitz, J. *Semin. Cell Dev. Biol.* **2000**, *11*, 53–60.

(36) Vérétout, F.; Delaye, M.; Tardieu, A. *J. Mol. Biol.* **1989**, *205*, 713–728.

(37) Bindels, J. G.; Koppers, A.; Hoenders, H. J. *Exp. Eye Res.* **1981**, *33*, 333–343.

(38) Slingsby, C.; Bateman, O. A. *Biochemistry* **1990**, *29*, 6592–6599.

(39) Ajaz, M. S.; Ma, Z.; Smith, D. L.; Smith, J. B. *J. Biol. Chem.* **1997**, *272*, 11250–11255.

(40) Nalini, V.; Bax, B.; Driessen, H.; Moss, D. S.; Lindley, P. F.; Slingsby, C. *J. Mol. Biol.* **1994**, *236*, 1250–1258.
PDB ID: 1BLB

(41) Broide, M. L.; Berland, C. R.; Pande, J.; Ogun, O. O.; Benedek, G. B. *Proc. Natl. Acad. Sci. U.S.A.* **1991**, *88*, 5660–5664.

(42) The UniProt Consortium *Nucl. Acids Res.* **2015**, *43*, D204–D212.

(43) Najmudin, S.; Nalini, V.; Driessen, H. P.; Slingsby, C.; Blundell, T. L.; Moss, D. S.; Lindley, P. F. *Acta Crystallogr. Sect. D - Biol. Crystallogr.* **1993**, *49*, 223–233.
      PDB ID: 4GCR

(44) Muschol, M.; Rosenberger, F. *J. Chem. Phys.* **1997**, *107*, 1953–1962.

(45) Piazza, R. *J. Cryst. Growth* **1999**, *196*, 415–423.

(46) Sear, R. P. *Curr. Opin. Colloid Interface Sci.* **2006**, *11*, 35–39.

(47) Gögelein, C.; Nägele, G.; Tuinier, R.; Gibaud, T.; Stradner, A.; Schurtenberger, P. *J. Chem. Phys.* **2008**, *129*, 085102.

(48) Tardieu, A. *Int. J. Biol. Macromol.* **1998**, *22*, 211–217.

(49) Thomson, J. A.; Schurtenberger, P.; Thurston, G. M.; Benedek, G. B. *Proc. Natl. Acad. Sci. U.S.A.* **1987**, *84*, 7079–7083.

(50) Schurtenberger, P.; Chamberlin, R. A.; Thurston, G. M.; Thomson, J. A.; Benedek, G. B. *Phys. Rev. Lett.* **1989**, *63*, 2064–2067.

(51) Tardieu, A.; Vérétout, F.; Krop, B.; Slingsby, C. *Eur. Biophys. J.* **1992**, *21*, 1–12.

(52) Hall, D.; Minton, A. P. *Biochim. Biophys. Acta* **2003**, *1649*, 127–139.

(53) Zhou, H.-X.; Rivas, G.; Minton, A. P. *Annu. Rev. Biophys.* **2008**, *37*, 375–97.

(54) Roosen-Runge, F.; Hennig, M.; Zhang, F.; Jacobs, R. M. J.; Sztucki, M.; Schober, H.; Seydel, T.; Schreiber, F. *Proc. Natl. Acad. Sci. U. S. A.* **2011**, *108*, 11815–11820.

(55) Grimaldo, M.; Roosen-Runge, F.; Zhang, F.; Seydel, T.; Schreiber, F. *J. Phys. Chem. B* **2014**, *118*, 7203–7209.

2
Protein purification

The proteins used in this project were purified from calf eyes obtained fresh as a by-product from a local slaughterhouse. The lenses (figure 2.1) were extracted from the eyes and the γ-rich nucleus separated from the cortical. Both parts

Figure 2.1: Calf eye lens. The nucleus of the lens is turbid, because it had been put on ice, an effect known as cold cataract.

were then, together with sodium acetate buffer at pH 4.5 (for the nuclear part) or phosphate buffer at pH 7.1 (for the cortical part), homogenized to break up the cell walls and release the proteins. To remove cell debris from the extracts, they were centrifuged at $18\,500g$ for 2 hours at $4°C$. Subsequently, the extracts were passed over chromatography columns to purify the proteins. The first part of this chapter describes the procedure followed to obtain γB-crystallin from the nuclear extract and the second part focuses on the purification of α- and βH-crystallin from the cortical part.

2.1 γB-crystallin

As it is most abundant in the lens nucleus (cf. section 1.3), γB-crystallin was purified from the nuclear extract by first passing it over a size-exclusion chromatography (SEC) column (Superdex 200 prep grade) using a salt-free 275 mM sodium acetate buffer at pH 4.5 as mobile phase, to separate γ-crystallin from α- and β-crystallin. SEC separates the proteins according to their size [1] and the resulting chromatogram is shown on the left-hand side of figure 2.2. Only the third peak, corresponding to a mixture of all γ-crystallins was collected. To
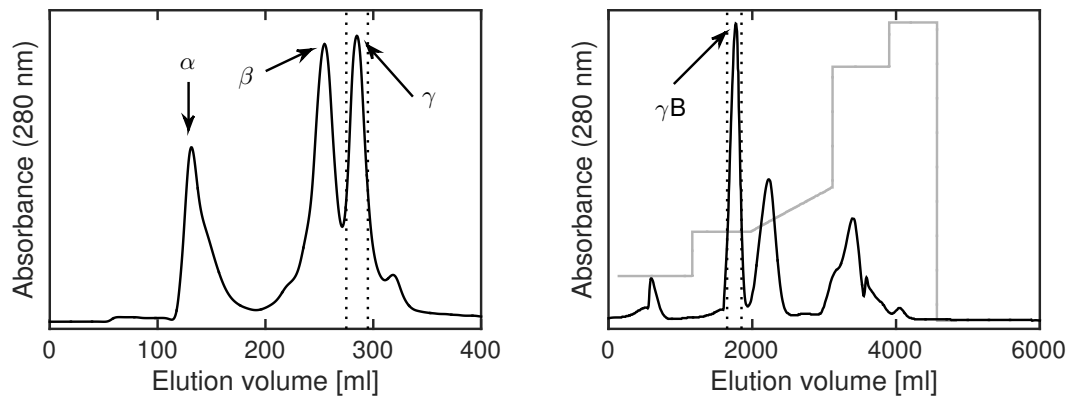
Figure 2.2: **Left:** Size-exclusion chromatogram of the nuclear extract. The dotted lines mark the part of the peak that was collected. **Right:** Cation-exchange chromatogram of the γ-crystallin mixture. The gray line shows the salt gradient used to elute the proteins and the dotted lines mark the part of the peak that was collected (corresponding to γB-crystallin).

extract γB-crystallin from the mixture, it was further purified using ion exchange chromatography (IEX) (SP Sepharose Fast Flow) and a 275 mM sodium acetate buffer at pH 4.8 with a 0–325 mM NaCl gradient to elute the proteins according to their pI [2]. The corresponding chromatogram is shown on the right-hand side of figure 2.2.

2.2 α- and βH-crystallin

α- and βH-crystallin were purified from the cortical extract by SEC on Superdex 200 prep grade using a 52.4 mM phosphate buffer at pH 7.1 as elution buffer. The corresponding chromatogram and the collected fractions are shown in figure 2.3.
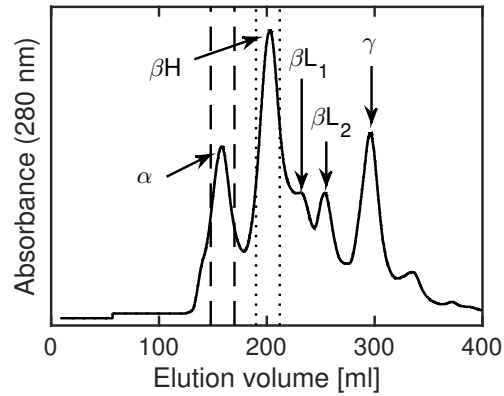
Figure 2.3: Size-exclusion chromatogram of the cortical extract. The dashed and the dotted lines mark the parts of the peaks that were collected.

References

(1) *Size Exclusion Chromatography - Principles and Methods*; GE Healthcare Bio-Sciences AB: 2014.
(2) *Ion Exchange Chromatography & Chromatofocusing - Principles and Methods*; GE Healthcare Bio-Sciences AB: 2010.

3

Scattering techniques

Scattering techniques are ideally suited to study both, structural and dynamic properties of protein solutions. The use of different types of radiation (light, X-rays or neutrons) leads to a large variety of scattering techniques, covering a broad range of time and length scales. They all build on the principle of irradiating a sample with a well characterized beam and subsequently analyzing the radiation scattered by the sample (figure 3.1). The main advantage of scattering techniques is that they are non-invasive and that they allow studying of bulk properties of solutions, which is not possible with techniques such as microscopy. The first part of this chapter deals with static scattering techniques, measuring the angular dependence of the scattered intensity, thus yielding information on the structure of the solution under investigation. The second part of the chapter is dedicated to dynamic techniques, utilizing the time-dependent intensity fluctuations of the scattered radiation to gain information on the dynamic behavior of the proteins in solution. I only give a brief description of the scattering techniques that I used, more details can be found for example in reference [1].
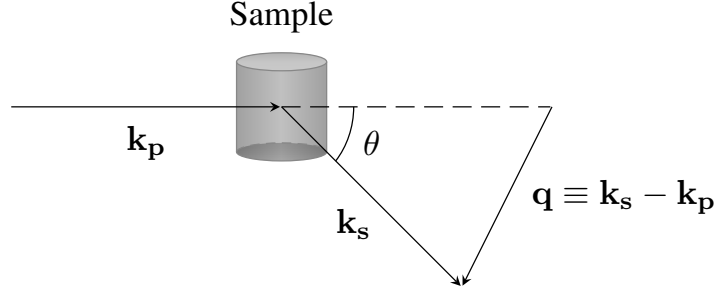
Figure 3.1: Schematic of a scattering experiment and definition of the scattering angle θ and the scattering vector $\mathbf{q}$, corresponding to the momentum transfer during the scattering event. $\mathbf{k_p}$ and $\mathbf{k_s}$ are the wave vectors of the primary and the scattered beam, respectively. Their magnitudes depend on the wavelength of the radiation λ and are given by $k = 2\pi/\lambda$.

3.1 Static scattering techniques

3.1.1 Theory

For (quasi-)elastic scattering techniques, i.e. techniques without (significant) energy transfer between the radiation and the sample during the scattering process, the wavelengths of the primary and the scattered beam are equal and hence $k_s = k_p = k$. The important quantities in a scattering experiment are the differential scattering cross-section

$$\frac{d\sigma}{d\Omega} = \frac{I_s L^2}{I_p} \tag{3.1}$$

which has units of (length)^2 and the differential scattering cross-section per unit sample volume

$$\frac{d\Sigma}{d\Omega} = \frac{1}{V}\frac{d\sigma}{d\Omega} \tag{3.2}$$

which has units of (length)$^{-1}$. I_p and I_s are the intensity of the primary and the scattered wave, respectively, L is the sample-detector distance and V is the volume of the particle.

Proteins in solution can be seen as extended particles, made up of multiple individual point scatterers, as depicted in figure 3.2. For each single point scatterer within such a particle, $d\sigma/d\Omega$ is given by

$$\frac{d\sigma}{d\Omega} = b^2 \tag{3.3}$$
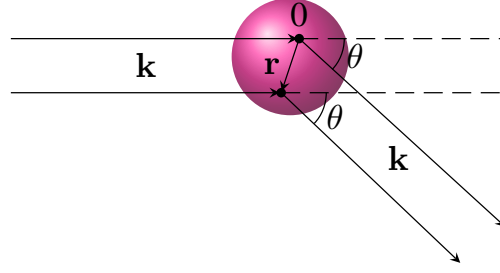
Figure 3.2: Scattering from two point scatterers within an extended particle (pink sphere), separated by a distance r.

where b describes the interaction between the radiation and the sample and therefore depends on the type of radiation used for the experiment. The total scattering of the particle, i.e. of all individual point scatterers, is expressed as a function of the excess scattering length density $\Delta\rho = \rho - \rho_{\text{solvent}}$ with ρ_{solvent} and $\rho = 1/V \sum_j b_j$ being the scattering length density of the solvent and the particle, respectively. b_j are the individual scattering lengths of the scattering centers.

3.1.2 Small-angle X-ray scattering (SAXS)

X-rays scatter on the electron clouds of atoms and hence, in this case, the scattering amplitude corresponds to the Fourier transform of the electron density, i.e. for large q-values, corresponding to small length scales, $d\sigma/d\Omega$ is q-dependent, with $q = (4\pi/\lambda)\sin(\theta/2)$, because the electron probability density varies from one atom to the other.

The left-hand side of figure 3.3 shows a schematic of a SAXS experiment with the q-dependent 2D scattering pattern on the detector. Spatially averaging this scattering pattern yields the q-dependent scattering intensity $I(q) \sim P(q)S(q)$, where the particle form factor $P(q)$ contains information about the size and the structure of the particle, i.e. it gives the scattering intensity from one particle due to intraparticle interference effects and the static structure factor $S(q)$ holds information about the particle correlations due to interactions. It is important to note that the resolution of a scattering experiment is $\sim 1/q$, i.e. at small q-values, large length scales (e.g. particles, macroscopic structures, interparticle effects) are probed and at large q-values, small length scales (e.g. inner structure of particles, intraparticle effets) are probed. At small q-values, $I(q)$ is thus dominated by $S(q)$ and at large q-values by $P(q)$. Experimentally, $P(q)$ corresponds to the concentration-normalized scattering intensity of a dilute sample where no particle interactions are present and

17

hence $S(q) \approx 1$. $S(q)$ of concentrated samples are then obtained by dividing their concentration-normalized measured scattering intensities $I(q)/c$ by $P(q)$. All scattering intensities have to be corrected for background from the capillary and the solvent, cosmic radiation, dark current and sample transmission.

A measure of the protein size, the radius of gyration R_g, giving the distribution of mass within the particle (root-mean square), can be extracted from $P(q)$ using the so-called *Guinier approximation*

$$P(q) \approx 1 - \frac{1}{3}q^2R_g^2 \approx \exp\left(-\frac{1}{3}q^2R_g^2\right), \tag{3.4}$$

valid for $q^2R_g^2 \ll 1$. It allows for a model-free determination of R_g of an object from small-q scattering.
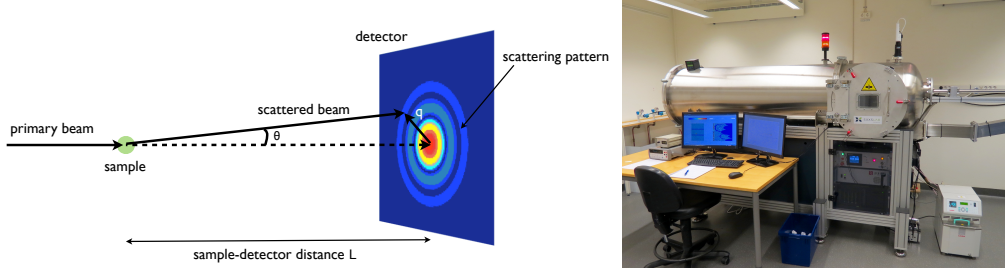
Figure 3.3: Schematic of a SAXS experimental setup (**left**) and Ganesha 300 XL SAXS System from SAXSLAB (**right**).

The SAXS experiments presented in this work were performed on a pinhole camera equipped with a high brilliance microfocus sealed tube, a Pilatus detector and a thermostated sample stage (Ganesha 300 XL SAXS System from SAXSLAB, shown on the right-hand side of figure 3.3). The detector is mounted on a motor, allowing to move it over 1400 mm, thus changing the sample-detector distance L. This leads to an accessible q-range of 0.003–2.5 Å^{-1}, i.e. length scales from some nanometers to hundreds of nanometers.

3.1.3 Static light scattering (SLS)

With light as radiation source, the contrast depends on the polarizability of the particles which is related to their refractive index n. Taking into account the size of the proteins under investigation here and the q-range covered with light scattering (0.001–0.003 Å^{-1}), the measured scattering intensity is q-independent

and can be written as

$$\Delta R_\theta \equiv \frac{d\Sigma}{d\Omega} = KcN_Ak_BT\kappa_T^{-1} \tag{3.5}$$

where ΔR_θ is the excess Rayleigh ratio, $\kappa_T \equiv \partial\Pi/\partial c$ is the osmotic compressibility and K is the optical constant or SLS contrast term, given by

$$K = \frac{1}{N_A}\frac{4\pi^2 n^2}{\lambda^4}\left(\frac{dn}{dc}\right)^2. \tag{3.6}$$

For interacting particles, the osmotic pressure Π can be expanded in c:

$$\Pi = N_Ak_BT\left(A_1c + A_2c^2 + A_3c^3 + \dots\right). \tag{3.7}$$

Equation (3.7) is known as *virial expansion* and the factors A_j are the virial coefficients. In second order, equation (3.5) can thus be rewritten as

$$\Delta R_\theta = Kc\left(\frac{1}{M_w} + 2A_2c\right)^{-1}. \tag{3.8}$$

The second virial coefficient A_2 which contains information about the particle-particle interactions is related to B_2 (more commonly used in literature), the second virial coefficient from the expansion in number density instead of c, through [2]

$$A_2 = B_2\frac{N_A}{M_w^2}. \tag{3.9}$$

Experimentally, ΔR_θ corresponds to the time-averaged scattering intensity, corrected for background scattering from the cell and solvent and normalized using a reference solvent. It can be used to determine B_2 and M_w.

For light scattering (LS) experiments, two different commercial goniometers (3D LS Spectrometer from LS Instruments AG and CGF-8F based compact goniometer system from ALV GmbH), as well as a homebuilt multiangle light scattering (MALS) instrument [3] were used (figure 3.4). The 3D LS Spectrometer from LS Instruments AG and the homebuilt MALS instrument implement the so-called 3D cross-correlation technique to suppress contributions from multiple scattering [4, 5]. The q-values accessed with LS are much smaller than those accessed with SAXS, i.e. the length scales covered with LS are larger.
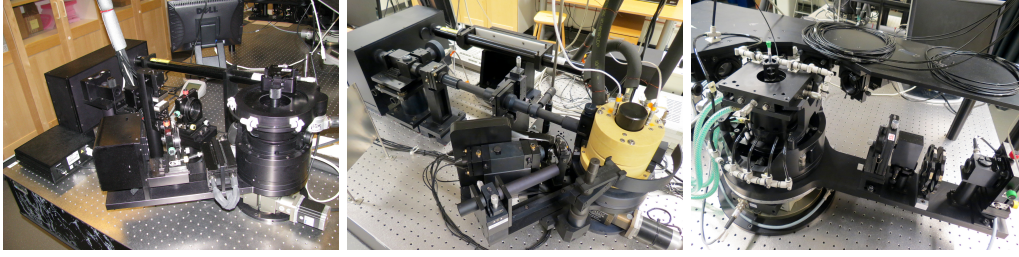
Figure 3.4: 3D LS Spectrometer from LS Instruments AG (**left**), CGF-8F based compact goniometer system from ALV GmbH (**center**) and the homebuilt MALS instrument (**right**).

3.2 Dynamic scattering techniques

3.2.1 Dynamic light scattering (DLS)

When a particle solution is irradiated with monochromatic coherent light, the beam is scattered in all directions and creates a grainy *speckle* pattern. Since the particles in the solution are not static, but move due to Brownian motion, the pattern they create on the detector, i.e. the scattering intensity, fluctuates in time. As opposed to SLS, in DLS this intensity is not time-averaged, but the time-dependence of the fluctuations is used to gain information on the diffusion of the particles in the solution. As the length scales covered by LS are one to two orders of magnitude larger than the size of the proteins that are the topic of this work, DLS probes the *collective* dynamics of the protein solutions.

Information on these collective dynamics is extracted from the experimentally determined normalized intensity autocorrelation function (ACF)

$$g_2(t) \equiv \frac{\langle I(0)I(t)\rangle}{\langle I(0)\rangle\langle I(t)\rangle} = \frac{\langle I(0)I(t)\rangle}{\langle I\rangle^2} \tag{3.10}$$

which is a comparison of the intensity I at time 0 and at a later time t. $g_2(t)$ can be related to the field ACF or intermediate scattering function (ISF) $g_1(t)$ through the *Siegert relation*

$$g_2(t) - 1 = A[g_1(t)]^2 \tag{3.11}$$

taking into account the intercept A which is a system-dependent correction factor. For polydisperse samples, $g_1(t)$ can be expressed by the so-called *cumulant*

expansion [6] which, in second order, is given by

$$g_1(t) = \exp{(-\Gamma_c t)}(1 + \frac{\mu_2}{2!}t^2) \tag{3.12}$$

where the decay constant Γ_c is related to the collective diffusion coefficient D_c through $D_c = \Gamma_c/q^2$ with $q = (4\pi n/\lambda)\sin{(\theta/2)}$ and the width of the distribution σ is related to the second moment μ_2. D_c is related to the dynamic correlation length ξ_d or apparent hydrodynamic radius $R_{h,\text{app}} \equiv \xi_d$, the radius of a theoretical sphere diffusing at the same rate as the protein under investigation, through the *Stokes-Einstein relation*

$$D_c = \frac{k_B T}{6\pi\eta(T)R_{h,\text{app}}} \tag{3.13}$$

where viscosity $\eta(T)$ is the solvent viscosity. For a freely diffusing non-interacting particle, equation 3.13 becomes

$$D_0 = \frac{k_B T}{6\pi\eta(T)R_{h,0}} \tag{3.14}$$

and is used to normalize D_c obtained at different temperatures T. Experimentally, the free diffusion coefficient D_0 is obtained by measuring increasingly dilute solutions and extrapolating the results to zero c.

For dynamically heterogeneous solutions, equation 3.12 usually fails to reproduce the ISFs and it is thus more common to instead apply a *Kohlrausch-Williams-Watts* stretched exponential function [7] of the form

$$g_1(t) = \exp\left[-(\Gamma_c t)^\beta\right], \quad 0 < \beta < 1. \tag{3.15}$$

For DLS, the same instruments were used as for SLS (figure 3.4).

3.2.2 Neutron spin echo (NSE)

Unlike X-rays which scatter on the electron cloud of atoms, the electrically neutral neutrons penetrate deeper into atoms and scatter on their nuclei. b depends unsystematically on the nucleus and strongly on the isotope in use. This effect is especially dramatic for hydrogen and deuterium where the former has a negative b, whereas for the latter, it is positive. Another important aspect of neutron scattering is that it has a *coherent*, as well as an *incoherent* contribution. Studying the coherent part of the scattering allows to obtain information on collective properties of the system, e.g. the solution structure. The incoherent

scattering, on the other hand, yields information about individual scatterers, such as their self-diffusion. The quasi-elastic NSE method, first described by Mezei [8] in 1972, makes use of the Larmor precession of the neutron's spin to investigate dynamics on length and time scales much smaller than those covered with DLS. As opposed to inelastic neutron scattering techniques, NSE spectrometers measure the energy transfer occuring during the scattering process and the ISF directly. Additionally, as their energy resolution is decoupled from the monochromatization of the primary beam, a broad wavelength band (10–20%) can be used, which leads to a relatively high flux [9, 10].

Experimentally, short-time diffusion coefficients can be extracted from the measured ISFs $f(q, t)$ by applying a single-exponential fit of the form

$$f(q, t) = \exp\left[-\Gamma_s(q)t\right] \tag{3.16}$$

to the initial part of the decay of the ISFs where the decay constant $\Gamma_s(q)$ is related to the short-time local diffusion coefficient $D_s(q)$ through $D_s(q) = \Gamma_s(q)/q^2$.

The experiments presented in this work were performed either on the IN15 spectrometer (figure 3.5) at the Institut Laue-Langevin (ILL) in Grenoble, France [9] or on the JCNS neutron spin-echo spectrometer J-NSE at the FRM II in Munich, Germany [10]. q-values between 0.01 Å^{-1} and 0.23 Å^{-1} were covered,

Figure 3.5: IN15 spectrometer at ILL in Grenoble, France.

corresponding to length scales on the order of the protein size, and Fourier times between 0.03 and 600 ns, allowing to probe the protein short-time dynamics on length scales corresponding to the nearest-neighbor distance. In order to avoid large background contributions from the solvent, protein solutions were prepared in D_2O, instead of H_2O, buffers.

References

(1) *Neutrons, X-rays and Light: Scattering Methods Applied to Soft Condensed Matter*; Lindner, P., Zemb, T., Eds.; Elsevier Science B.V.: 2002.

(2) Wolf, M.; Roosen-Runge, F.; Zhang, F.; Roth, R.; Skoda, M. W. A.; Jacobs, R. M. J.; Sztucki, M.; Schreiber, F. *J. Mol. Liq.* **2014**, *200*, 20–27.

(3) Moitzi, C.; Vavrin, R.; Bhat, S. K.; Stradner, A.; Schurtenberger, P. *J. Colloid Interface Sci.* **2009**, *336*, 565–574.

(4) Schätzel, K. *J. Mod. Opt.* **1991**, *38*, 1849–1865.

(5) Urban, C.; Schurtenberger, P. *J. Colloid Interface Sci.* **1998**, *207*, 150–158.

(6) Frisken, B. J. *Appl. Opt.* **2001**, *40*, 4087–4091.

(7) Klafter, J.; Shlesinger, M. F. *Proc. Natl. Acad. Sci. U. S. A.* **1986**, *88*, 848–851.

(8) Mezei, F. *Z. Physik* **1972**, *255*, 146–160.

(9) Farago, B. *Physica B* **1999**, *267-268*, 270–276.

(10) Holderer, O.; Monkenbusch, M.; Schätzler, R.; Kleines, H.; Westerhausen, W.; Richter, D. *Meas. Sci. Technol.* **2008**, *19*, 034022 (6pp).

Part II

RESULTS

4

Individual proteins

In this chapter, I will focus on aqueous solutions of the individual eye lens proteins and describe their interactions, solution microstructure and dynamics on collective and local length scales. I will point out different arrest scenarios that emerge in these systems, depending on the type of protein-protein interactions. This chapter is an overview of the main results, described in more detail in the different papers. It is divided into three sections, each dedicated to a different protein and all experiments described here were performed on proteins in 52.4 mM phosphate buffer at pH 7.1, i.e. close to physiological pH.

In order to understand the effect that different interaction potentials have on protein solution dynamics, it is important to establish the interactions governing the solution, prior to investigating the dynamic properties of the solutions. Colloidal particles with short-range attractions are known to exhibit a range of different phases, depending on the strength of the attraction U_a and the total volume fraction ϕ_{tot}, as depicted in figure 4.1. In the following three sections, I will explain how the interaction potentials of the individual crystallins were determined and how they fit into this phase diagram.
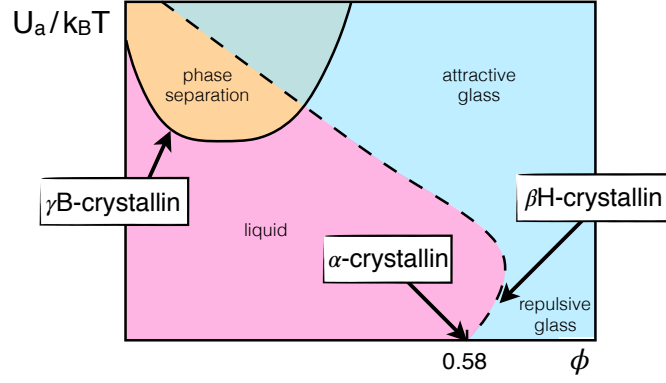
Figure 4.1: Phase diagram of eye lens proteins (adapted from the generic state diagram of colloidal particles with short-range attractions reported in reference [1]). Shown are the glass line (— —) and the metastable liquid-liquid coexistence curve (binodal, ——). Also indicated are the locations of the three main components of the eye lens in this phase diagram, according to their interaction potentials.

4.1 α-crystallin

To establish the solution microstructure, we used SAXS to obtain the static structure factor $S(q)$ at varying ϕ (with $\phi = c \cdot v$, where c is the concentration and v the voluminosity of the protein), as shown in figure 4.2a. The main features of $S(q)$ of α-crystallin are a strong monotonic reduction of its value in the forward direction, $S(0)$, related to the osmotic compressibility κ_T (figure 4.2b), and a developing first peak, corresponding to the average distance between the proteins in solution, d^*. Upon increasing c, the location of this peak, $q^* \sim 1/d^*$, shifts towards larger q (inset in figure 4.2a), as the average distance between the proteins in solution decreases. The proteins thus move closer together when the solution becomes more crowded. Both features are typically observed in HS solutions. As shown in **Paper I**, the concentration-dependence of $S(0)$ is indeed in agreement with predictions for monodisperse and polydisperse HSs. The entire q-range of the structure factors can however only be reproduced assuming a polydispersity of about 20%. This model yields $v = 1.7$ ml/g and a number-average diameter of 15 nm. Compact globular proteins typically have a voluminosity of $v \approx 0.7$ ml/g. The comparatively large value obtained for α-crystallin is owed to the fact that these are non-compact multi-subunit proteins with rather loosely assembled subunits. Polydispersity prevents crystallization of the protein solution and ensures that it remains in a liquid-like state until it undergoes a glass transition at large ϕ. To exactly locate this glass transition, we have investigated the protein dynamics on different length scales, starting with the collective diffusive behavior on large length scales, probed by DLS.
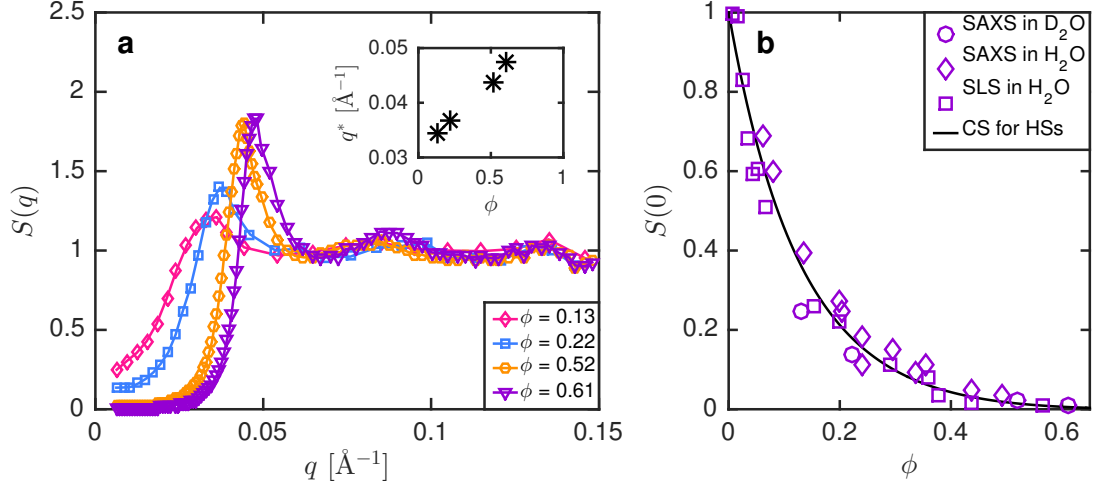
Figure 4.2: **a**: Structure factors of α-crystallin in D_2O at varying ϕ. Inset: Location of the nearest-neighbor peak as a function of ϕ. **b**: Value of $S(q)$ in the forward direction from SLS and SAXS in D_2O and H_2O as a function of ϕ, together with the Carnahan-Starling (CS) prediction for colloidal hard spheres (HSs), $S_{CS}(0) = (1-\phi)^4/[(1+2\phi)^2 + \phi^3(\phi-4)]$ [2].

Under dilute conditions, we find ISFs exhibiting a single exponential relaxation, as expected for a simple fluid. The diffusion coefficient, obtained from the ISFs using equation 3.12, shows the same ϕ-dependence as colloidal HSs and can be extrapolated to zero concentration to obtain D_0 and the corresponding $R_{h,0} = 9.6$ nm. Upon increasing ϕ, a two-step decay begins to emerge, caused
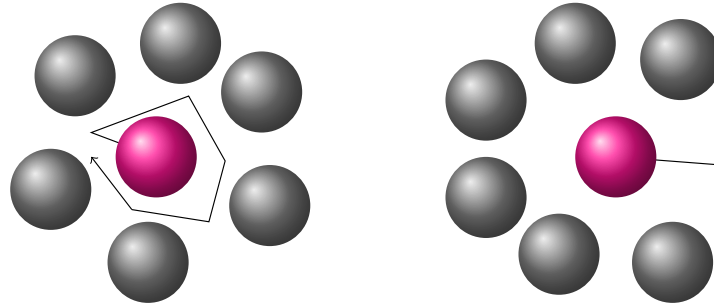
Figure 4.3: **Left:** α-crystallin protein (in pink) rattling within its cage of nearest-neighbors, shown in gray. (Note that the proteins forming the cage are also trapped in cages of nearest neighbors and are diffusing within them. For simplicity's sake, their cages and trajectories are however not shown here). **Right:** The same α-crystallin diffusing out of the cage after local rearrangements of the surrounding proteins have created an opening.

by the cage that surrounding particles form around each protein in a dense solution. The initial decay of the ISFs is called β-relaxation and can be attributed to the diffusion of proteins within their nearest-neighbor cage (left-hand side

of figure 4.3). Eventually, collective rearrangements in the solution lead to an opening of this cage, allowing the trapped particle to escape (right-hand side of figure 4.3), thus leading to a decay of the plateau at large delay times (also known as α-relaxation). As ϕ increases, it takes increasingly long for the nearest-neighbor cage to open, pushing the α-relaxation to longer times, thus leading to a slowing down of the long-time solution dynamics. Up to $\phi = 0.58$, the ISFs still fully decay, i.e. the protein solutions are in a liquid-like state. At $\phi > 0.58$, this is however not the case anymore and the ISF reaches a finite plateau value, a signature of the macroscopic arrest of the sample. A power law fit to the slow relaxation time, defined as the time when the ISF has reached a value of 0.25, yields the exact volume fraction at which this macroscopic arrest transition takes place: $\phi_{\mathrm{arr}} = 0.585$, in good agreement with the value obtained for colloidal HSs.

Further insight into the dynamics governing concentrated α-crystallin solutions can be obtained from measurements of the local dynamics on length scales corresponding to d^*, probed with NSE. The corresponding normalized diffusion coefficients are shown in figure 4.4a. As described in **Paper II** and in more detail
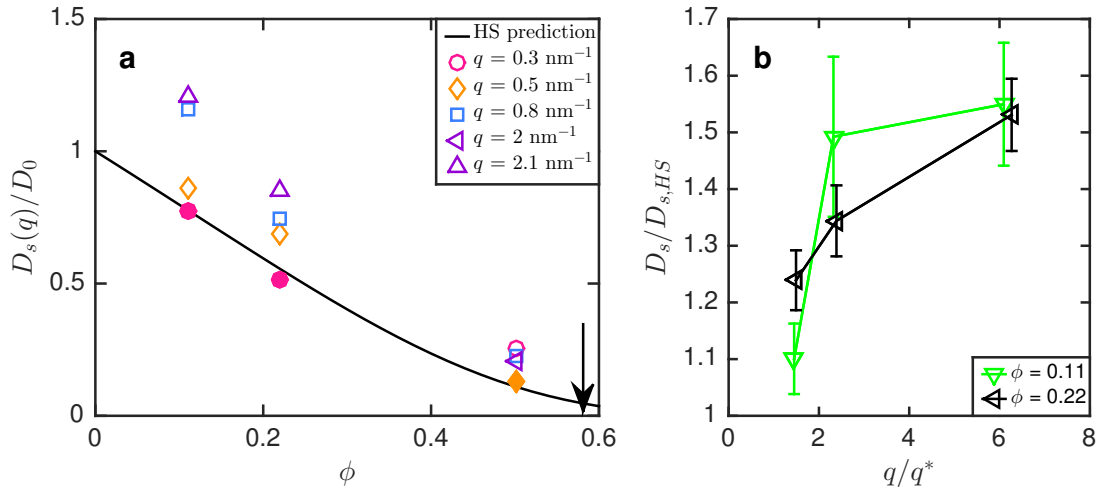
Figure 4.4: **a**: Normalized short-time local diffusion coefficients of α-crystallin in D_2O at varying q. Filled symbols show the data closest to q^* (shown in the inset of figure 4.2a). The theoretical prediction for the short-time local diffusion of colloidal HSs was taken from reference [3]. Also shown as an arrow is the volume fraction of macroscopic arrest. **b**: Deviation from HS behavior as a function of the distance to q^*. D_s corresponds to the data points and $D_{s,\mathrm{HS}}$ to the solid line shown in a.

in **Paper III**, in the short-time limit on which we focused our study, proteins do not have time to diffuse over long enough distances for caging effects to become

relevant, i.e. in this time window, they can be neglected. As can be seen from figure 4.4a, $D_s(q^*)/D_0$ of α-crystallin (filled symbols) decreases over a rather large range of ϕ values, following the theoretical prediction for HSs. From this, we can infer that at $\phi \approx 0.58$, where the caging by neighboring particles leads to macroscopic arrest of the α-crystallin solution, the individual proteins remain locally mobile and can still 'rattle' in their nearest-neighbor cages. At q-values larger than q^*, i.e. at distances smaller than the average distance between proteins in solution, the normalized local diffusion coefficients of α-crystallin increase beyond the values predicted for HSs (figure 4.4). Increasing q, we look at increasingly smaller distances and at $q = 0.21$ Å^{-1}, we look at distances corresponding to the nearest-neighbor distance of γB-crystallin (cf. section 4.3). Taking into account the fact that the size of the subunits forming α-crystallin is similar to the size of γB-crystallin (cf. section 1.3), this means that at $q = 0.21$ Å^{-1}, we also look at distances similar to the size of these subunits. The increase in $D_s(q)/D_0$ is thus most likely due to rotational and translational diffusion, as well as internal dynamics, i.e. the motion of the subunits which we start to resolve as we 'zoom into the protein'.

4.2 βH-crystallin

Paper IV is dedicated to βH-crystallin. The first part describes the characterization of the protein as a colloidal particle. We find that in order to determine the type of interactions governing the solutions, we have to compare data sets obtained by different scattering techniques (SLS, SAXS and DLS). $S(q)$ and $S(0)$, shown in figure 4.5, exhibit the typical features found for HSs already described in the previous section. As opposed to the case of α-crystallin, the nearest-neighbor peak of βH-crystallin is however much less well-defined, signature of larger polydispersity in the system. The concentration-dependence of the normalized collective diffusion coefficient (or rather the absence of it) does however not resemble that of HSs and can only be explained by additional weak short-range attractions of the order of $0.5 k_B T$ in the system. As a measure of the protein size, we obtain $R_{h,0} = 6.4$ nm from a cumulant analysis (equation 3.12) of the inital parts of the ISFs from DLS (shown in figure 4.6a), of samples at low to intermediate concentrations (up to 160 mg/ml).

The second part of the manuscript describes the protein dynamics on different length scales, starting with the collective dynamics. Comparable to α-crystallin, a two-step decay develops in the ISFs of βH-crystallin at concentrations above
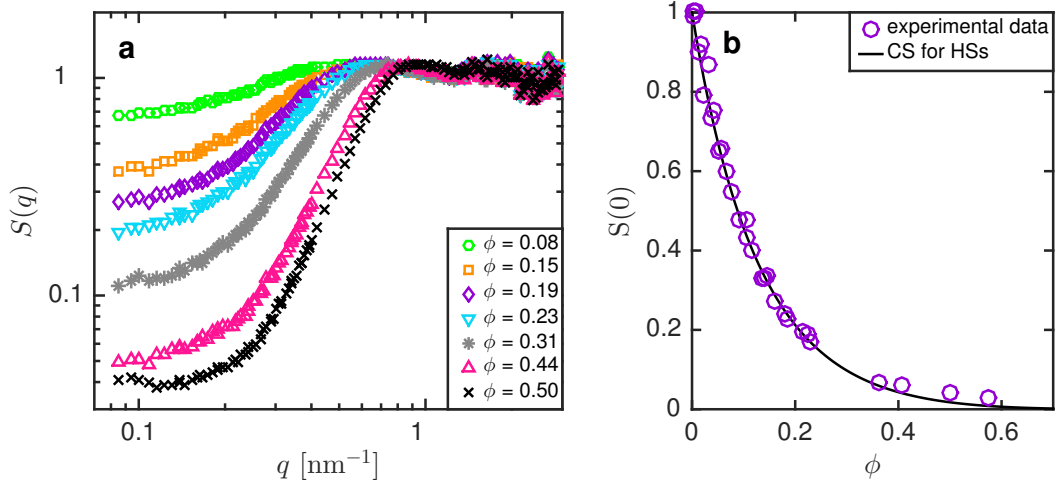
Figure 4.5: **a**: Structure factors of βH-crystallin in H_2O at T = 25°C. **b**: Value of $S(q)$ in the forward direction from SLS at T = 25°C (in H_2O), together with the Carnahan-Starling (CS) prediction for colloidal HSs.

about 200 mg/ml (cf. figure 4.6a), a clear signature of the proximity of an arrest line caused by caging by neighboring particles, i.e. macroscopic arrest of solutions of βH-crystallin is dominated by excluded volume (hard core) interactions of the proteins. From a power law fit to the corresponding normalized slow decay time, combined with data from DLS-based microrheology, we estimate the arrest transition to take place at $c_{arr} = (425 \pm 14)$ mg/ml. The weak short-range attractions and the high polydispersity push macroscopic arrest to larger ϕ compared to pure HSs. We therefore assume that the arrest transition takes place between $\phi_{arr} = 0.58$ (the value found for monodisperse HSs) and 0.67 (random close-packing for polydisperse particles) and use those values to obtain an estimate of the voluminosity. We find $v = (1.47 \pm 0.11)$ ml/g and correspondingly $\phi_{arr} = 0.62 \pm 0.05$. This voluminosity is again much larger than that of compact proteins, compatible with the fact that βH-crystallin is a multisubunit protein, with a slightly more compact structure than α-crystallin. On short length scales, we find that the weak short-range attractions lead to a deviation from HS behavior and cause a deceleration of the local dynamics at intermediate to high ϕ compared to a system where only caging by neighboring particles affects protein diffusion, as shown in figure 4.6b.
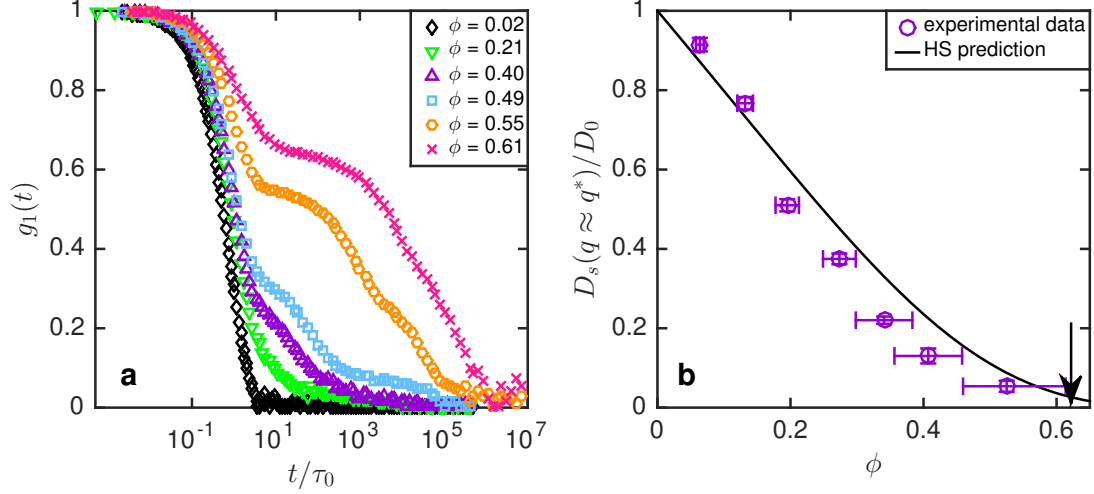
32

Figure 4.6: **a**: Intermediate scattering functions of βH-crystallin in H_2O from DLS at $T = 25°C$. The time axis was normalized with the decay time of a non-interacting particle $\tau_0 = (D_0 q^2)^{-1}$. **b**: Effective short-time local diffusion coefficient of βH-crystallin in D_2O on length scales corresponding to the average nearest-neighbor distance d^* from NSE at $T = 35°C$. The arrow marks the volume fraction of macroscopic arrest. The theoretical prediction for the short-time local diffusion of colloidal HSs was taken from reference [3].

4.3 γB-crystallin

Papers II, **III** and **V** describe the complex dynamics of concentrated γB-crystallin solutions, linked to the weak short-range attractions ($U_a \approx 1 k_B T$) between the proteins, and elucidate the underlying mechanisms.

When lowering the temperature of a solution of γB-crystallin, the temperature-dependent attractions will eventually cause it to become unstable and phase-separate. The corresponding metastable liquid-liquid phase boundary, or binodal, and the spinodal in D_2O, as shown in figure 4.10, have a critical volume fraction $\phi_c = 0.15 \pm 0.014$ and a critical temperature $T_c \approx 19°C$. The attractive interactions in the system are also reflected in the static structure factors where they lead to a q-independent nearest-neighbor peak, located at $q^* \approx 0.2\ \text{Å}^{-1}$, as shown in the inset of figure 4.7, and to a strong increase of $S(0)$ with a maximum around ϕ_c which becomes more pronounced at low temperatures (cf. figure 4.7a-c). As shown in **Paper V**, $S(0)$ can be separated into a temperature-independent non-critical background ($\times$ in figure 4.7d) which follows the CS prediction for HSs, i.e. is due to excluded volume interactions, and a strongly temperature-dependent critical component (colored symbols in figure 4.7d). The ϕ-dependence of $S(0)$ can be quantitatively reproduced using
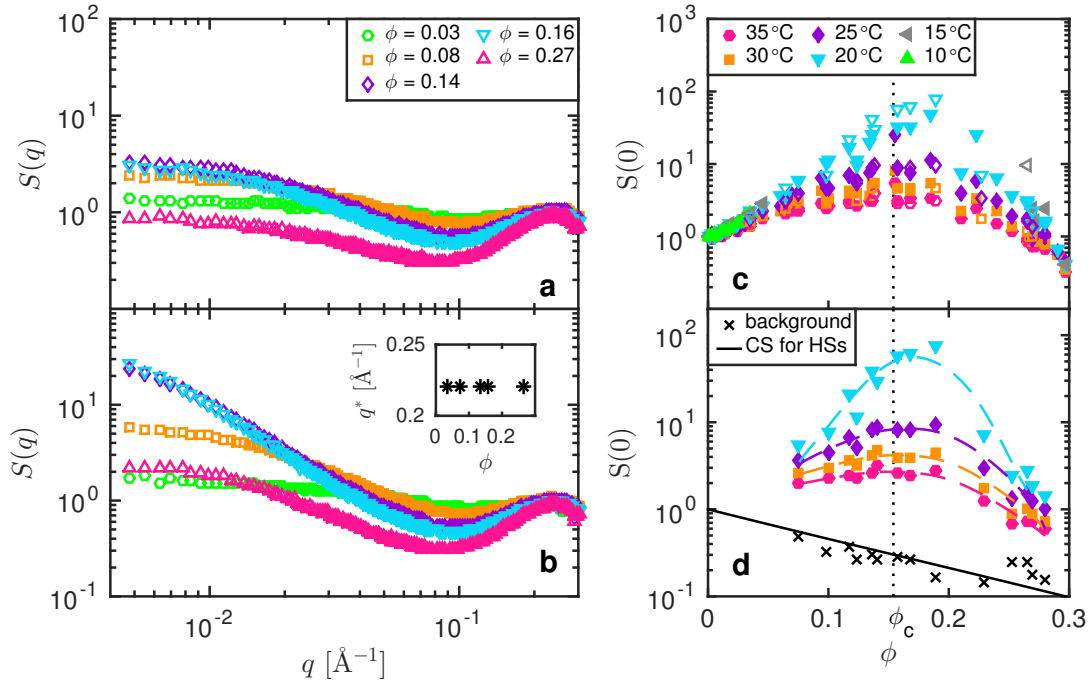
Figure 4.7: **Left**: Structure factors of γB-crystallin in D$_2$O at $T = 35°$C (**a**) and $T = 20°$C (**b**). Inset: Location of the nearest-neighbor peak as a function of ϕ. **Right**: Value of $S(q)$ in the forward direction from SLS (filled symbols) and SAXS (open symbols). **c**: Total $S(0)$, **d**: T-independent non-critical background, following the CS prediction for colloidal HSs and T-dependent critical component of $S(0)$. The dashed lines serve as guides to the eye and the dotted line marks the critical volume fraction.

a model of short-range attractive hard ellipsoids (cf. **Paper V** for more details).

The proximity of a critical point does not only have an impact on the solution structure, but also on the collective dynamics, causing what is known as critical slowing down around ϕ_c linked to large scale concentration fluctuations, as discussed in **Paper V** and shown in figure 4.8a. Moreover, the protein-protein

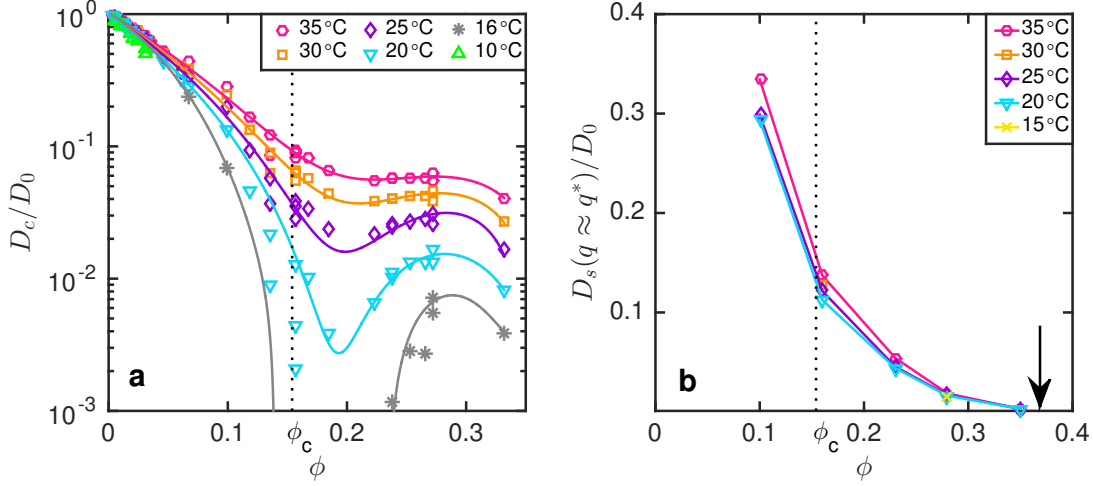Figure 4.8: **a**: Normalized collective diffusion coefficient of γB-crystallin in D_2O from DLS at varying T. The lines serve as guides to the eye **b**: Normalized short-time local diffusion coefficient on length scales corresponding to the nearest-neighbor distance from NSE at different T. The dotted line marks the critical volume fraction and the arrow marks the volume fraction of macroscopic arrest.

attractions lead to a glass line at large ϕ, located by performing temperature quenches deep into the unstable region of the phase diagram and determining the concentration of the dense phase after liquid-liquid phase separation. The competition between these two phenomena (critical slowing down and dynamical arrest) at intermediate to large volume fractions and low temperatures leads to a logarithmic, rather than exponential, decay of structural relaxations in the system, captured by DLS, as shown in figure 4.9. Additionally, at large ϕ (figure 4.9c), a shoulder in the ISFs emerges at large decay times, most likely due to slowing down of the system dynamics because of the formation and decay of transient clusters induced by the short-range attractions. Using DLS alone, it is thus clearly not possible to disentangle critical slowing down and dynamical arrest. This hurdle can be overcome by using NSE to look at protein dynamics on distances corresponding to the nearest-neighbor distance d^*. $D_s(q^*)$ does indeed remain unaffected by critical fluctuations, exhibits only a small T-dependence and decays fully over a much smaller ϕ-range than in the case of α- and βH-crystallin
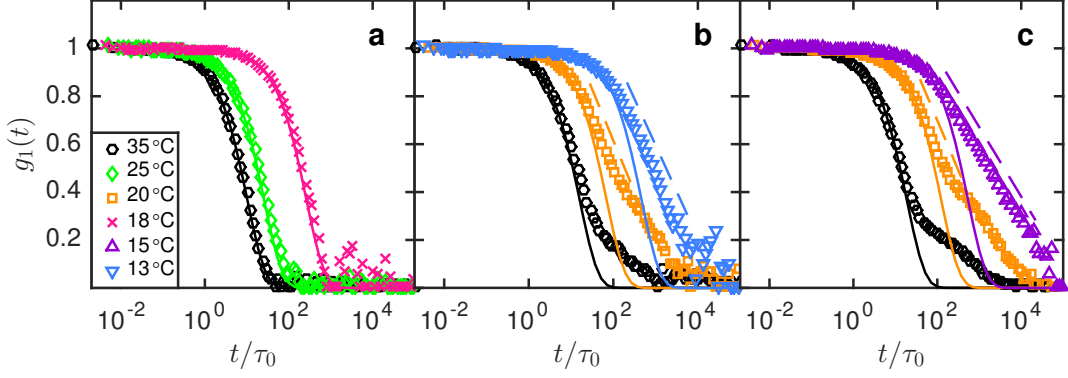
Figure 4.9: ISFs of γB-crystallin in D_2O from DLS at $\phi = 0.16$ (**a**), 0.27 (**b**) and 0.33 (**c**). Also shown are exponential (———) and logarithmic fits (– – , offset from the actual data for clarity).

(cf. figure 4.8b). As opposed to critical slowing down, dynamical arrest at large ϕ is thus a true arrest on all length scales. As shown in **Paper II**, the enormous slowing down found in γB-crystallin solutions cannot be explained by simple centrosymmetrical attractions, but patchiness has to be taken into account. The presented model with two attractive patches on the protein surface, diametrically opposite of each other, allows for a qualitative reproduction of the experimental data. While an even less coarse-grained model taking into account more of the actual protein structure, such as hydrophobic patches on the surface, will be necessary to quantitatively reproduce the experimental data, this first step clearly shows the importance of anisotropic interactions for the protein dynamics, as they lead to the formation of transient clusters that induce a complete arrest on all length scales at a volume fraction of only 35%.

4.3.1 Isotope effect

In **Paper VII**, we study the effect of buffer hydrogen isotope content on the phase behavior and thermodynamic properties of γB-crystallin. We find that the shape of the binodal and spinodal are independent of buffer isotope content and that the critical temperature shifts according to

$$T_c \, [K] = 0.16 \cdot \text{vol}\%(D_2O) + 276 \tag{4.1}$$

where $\text{vol}\%(D_2O)$ is the volume percentage of deuterium in the buffer. We show that the extended law of corresponding states (ELCS) is valid and that, using the critical temperature as a scaling factor, the reduced second virial coefficients $b_2 = B_2/B_2^{\text{HS}}$, the phase diagrams and $S(0)$ of solutions with

different proportions of D$_2$O superimpose, as shown in figure 4.10. Results
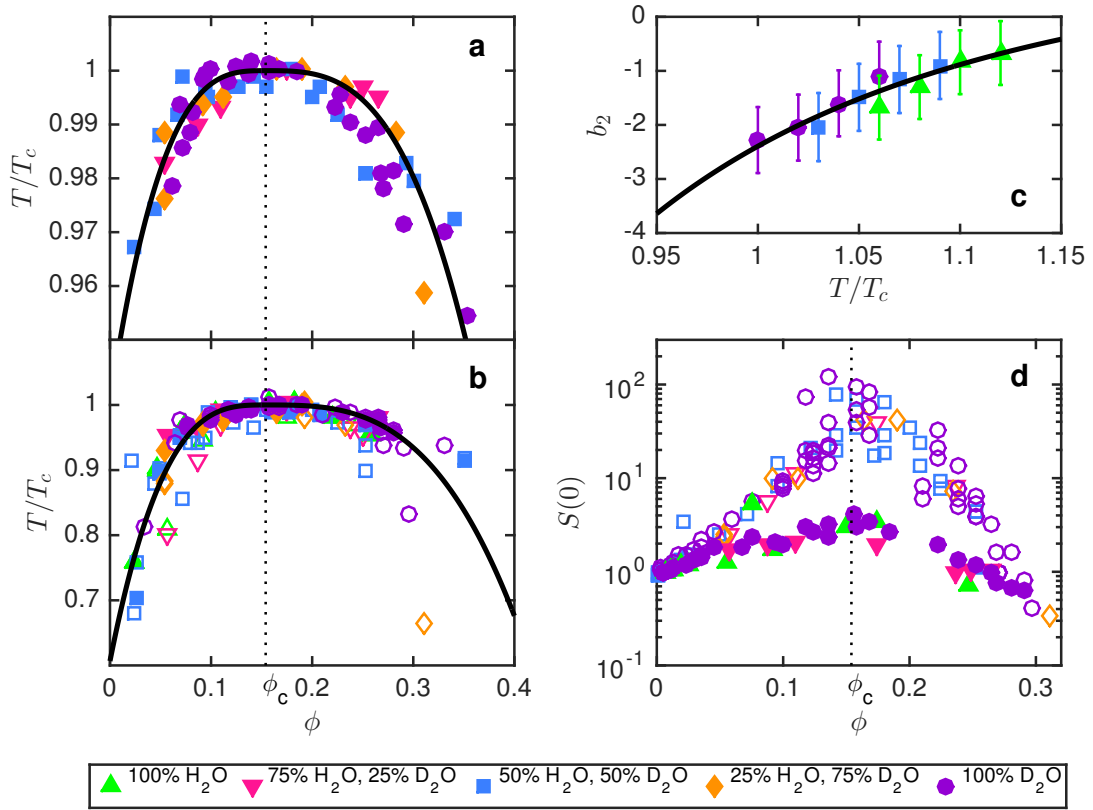

Figure 4.10: Binodal (**a**) and spinodal (**b**) of γB-crystallin in buffers with varying hydrogen isotope content, normalized with the critical temperature T_c. Open and filled symbols in **b** correspond to SLS and SAXS data, respectively. **c**: Reduced second virial coefficient $b_2 = B_2/B_2^{\text{HS}}$ as a function of reduced temperature. **d**: $S(0)$ from SLS at $T/T_c \approx 1.06$ (filled symbols) and $T/T_c \approx 1$ (open symbols).

obtained for buffers with different hydrogen isotope content are thus generally valid, provided that T_c is taken into account. In our case, this specifically means that our findings, obtained using D$_2$O buffer, are important for physiological solutions (containing hydrogen instead of deuterium).

References

(1) Gibaud, T.; Mahmoudi, N.; Oberdisse, J.; Lindner, P.; Pedersen, J. S.; Oliveira, C. L. P.; Stradner, A.; Schurtenberger, P. *Faraday Discuss.* **2012**, *158*, 267–284.

(2) Carnahan, N.; Starling, K. *J. Chem. Phys.* **1969**, *51*, 635–636.

(3) Banchio, A. J.; Nägele, G. *J. Chem. Phys.* **2008**, *128*, 104903.

5

Protein mixtures

To approach the conditions found in the ocular lens, we also studied binary mixtures of the individual proteins, again using a combination of different scattering methods to gain a better understanding of the solution dynamics and the interactions that influence them. This chapter is divided into two parts, the first one dedicated to $\alpha/\gamma B$ mixtures and the second one to $\beta H/\gamma B$ mixtures. All experiments were again performed in 52.4 mM phosphate buffer at pH 7.1. The results presented here are far from complete, but serve as a starting point for further investigation in the future.

5.1 $\alpha/\gamma B$ mixtures

Paper VI presents a study of the short-time dynamics of $\alpha/\gamma B$ mixtures on different length scales, using a combination of DLS and NSE. We find that the normalized collective diffusion coefficient of the mixtures, represented as a function of the effective volume fraction of γB-crystallin, mimics that of pure γB-crystallin with a strong slowing down around the critical volume fraction, as shown in figure 5.1a. The presence of α-crystallin in the mixtures leads to a faster collective motion, compared to mixtures of pure γB at the same effective volume fraction. This effect can be explained by the fact that for repulsive particles, such as α-crystallin, $D_c/D_0 > 1$, whereas for γB, $D_c/D_0 < 1$. As DLS probes
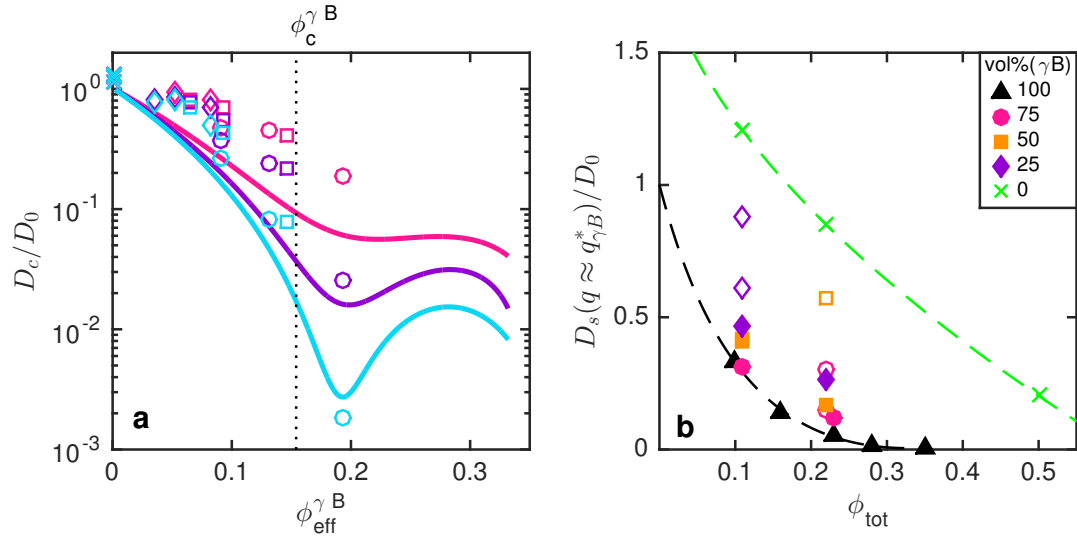
Figure 5.1: **a**: Normalized short-time collective diffusion coefficient of $\alpha/\gamma B$ mixtures in D$_2$O from DLS at $T = 35°C$, $25°C$ and $20°C$ as a function of the effective volume fraction of γB. ——: 100 vol% γB (same data as in figure 4.8a), ○: 25 vol% α, 75 vol% γB, □: 50 vol% α, 50 vol% γB, ◇: 75 vol% α, 25 vol% γB. The dotted line marks the critical volume fraction of γB. **b**: Normalized short-time local diffusion coefficient on length scales corresponding to the nearest-neighbor distance of γB from NSE as a function of the total volume fraction of proteins in the mixture. – – and – – are guides to the eye, tracing $D_s(q^*_{\gamma B})/D_0$ of pure γB-crystallin (same data as in figure 4.8b) and pure α-crystallin (same data as in figure 4.4a), respectively. Filled symbols correspond to experimental data, open symbols to hypothetical mixtures with the same composition without specific mutual α–γB interactions.

40

large length scales, a large number of proteins, α as well as γB, contributes to the measured collective diffusion coefficient. At total volume fractions of about 20%, we start to observe a deviation from single exponential decay of the ISFs, similar to the effect described in section 4.3 for γB-crystallin. We assume that this effect is again due to a competition between critical slowing down and dynamical arrest, underlined by NSE data (figure 5.1b) where we observe a slowing down of the short-time diffusion of the proteins on length scales corresponding to the average nearest-neighbor distance of γB-crystallin with increasing ϕ_{tot}. Additionally, we show that the mutual attractions between α and γB lead to further slowing down of the protein dynamics, compared to hypothetical mixtures of proteins without specific mutual interactions (open symbols in figure 5.1b). In Paper II, we showed for pure γB-crystallin that such a tremendous slowing down can only be explained by patchy γB–γB attractions, leading to the formation of transient space-spanning clusters, as shown schematically on the left-hand side of figure 5.2. The mixture dynamics
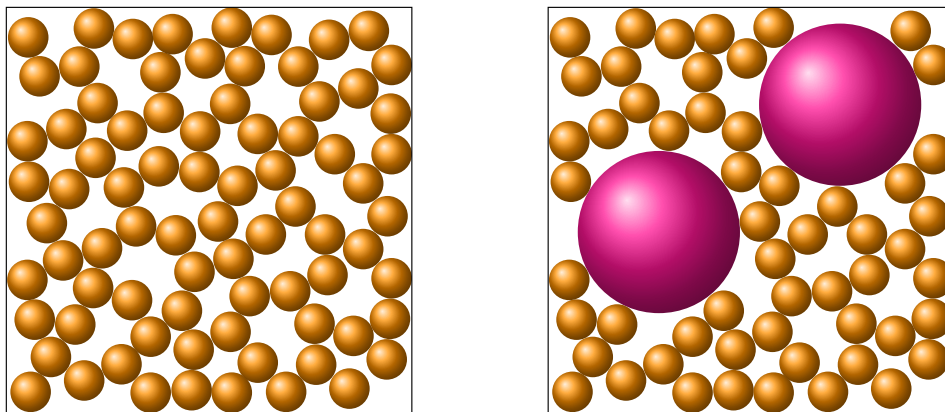

Figure 5.2: **Left**: Schematic of a transient cluster in a solution of pure γB-crystallin (orange), induced by short-range patchy attractions. **Right**: Schematic of a transient cluster in a mixture of α (pink) and γB-crystallin (orange).

are clearly also dominated by such anisotropic interactions and we can conjecture that the mutual α–γB attractions are also patchy and enhance the formation of transient clusters, as depicted on the right-hand side of figure 5.2. However, computer simulations will be necessary to establish whether this really is the case and how exactly mutual α–γB attractions affect the short-time local dynamics of the mixtures.

5.2 $\beta H/\gamma B$ mixtures

We also studied binary mixtures of β- and γB-crystallin, following the approach described in detail in Paper VI. The short-time collective and local dynamics of the different mixtures are shown in figure 5.3, as a function of the effective volume fraction ϕ_{eff} of γB-crystallin, given by

$$\phi_{\text{eff}}^{\gamma B} = \frac{\text{vol}\%(\gamma B)\,\phi_{\text{tot}}}{100 - \text{vol}\%(\beta H)\,\phi_{\text{tot}}\,(v_{\beta H}^{\text{eff}}/v_{\beta H})} \tag{5.1}$$

where $v_{\beta H} = 1.47$ ml/g is the voluminosity of βH-crystallin and $v_{\beta H}^{\text{eff}} = v_{\beta H}\left[(R_{\beta H} + R_{\gamma B})^3/R_{\beta H}^3\right] = 3.2$ ml/g is its effective voluminosity, taking into account the depletion shell around it, linked to the difference in size between the two proteins in the mixtures. It was calculated based on the radii of
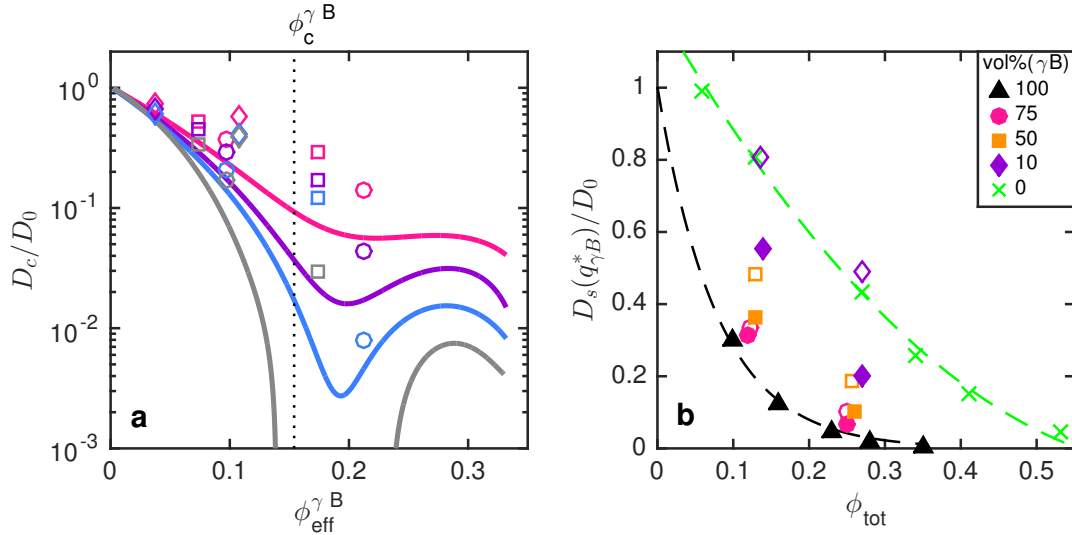

Figure 5.3: **a**: Normalized short-time collective diffusion coefficient of $\beta H/\gamma B$ mixtures in D$_2$O from DLS at $T = 35°\text{C}$, $25°\text{C}$, $20°\text{C}$ and $17°\text{C}$ as a function of the effective volume fraction of γB. ——: 100 vol% γB (same data as in figure 4.8a), ○: 25 vol% βH, 75 vol% γB, □: 50 vol% βH, 50 vol% γB, ◇: 75 vol% βH, 25 vol% γB. The dotted line marks the critical volume fraction of γB. **b**: Normalized short-time local diffusion coefficient on length scales corresponding to the nearest-neighbor distance of γB from NSE as a function of the total volume fraction of proteins in the mixture. – – and – – are guides to the eye, tracing $D_s(q_{\gamma B}^*)/D_0$ of pure γB-crystallin (same data as in figure 4.8b) and pure βH-crystallin, respectively. Filled symbols correspond to experimental data, open symbols to hypothetical mixtures with the same composition without specific mutual βH–γB interactions.

the proteins ($R_{\beta H} = 6$ nm and $R_{\beta H} = 1.8$ nm). We see that the existence of a critical point again leads to critical slowing down of the collective dynamics,

probed by DLS. Moreover, the presence of βH-crystallin in the solutions leads to overall larger D_c/D_0 compared to pure γB-crystallin, due to the fact that at the volume fractions considered here, D_c/D_0 of βH-crystallin ≈ 1, independently of ϕ. The short-time local dynamics on distances of the order of the average nearest-neigbor distance of γB-crystallin, probed by NSE, exhibit a strong slowing down with increasing ϕ_{tot} (cf. figure 5.3b), leading to a stretching of the DLS correlation functions, as shown in figure 5.4. To evaluate whether
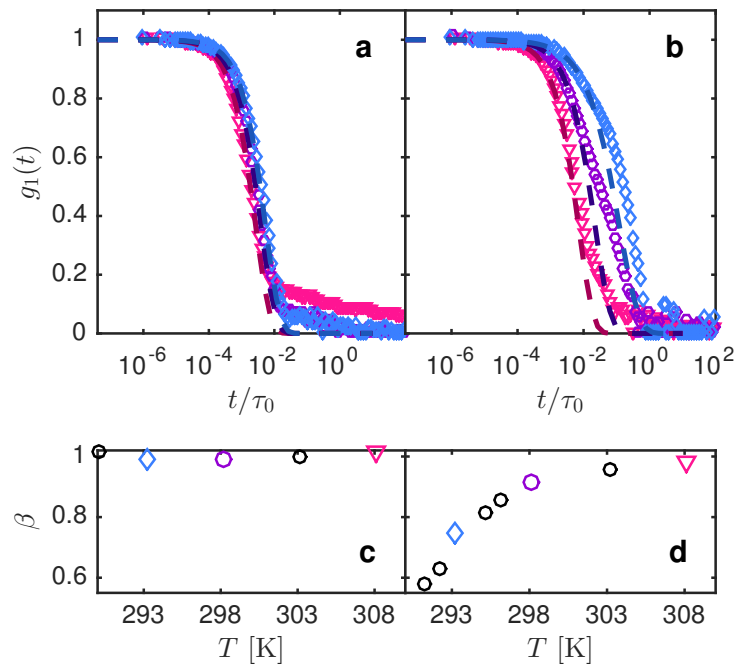

Figure 5.4: **a**, : Measured ISFs of mixtures with 25 vol% βH and 75 vol% γB at $\theta = 90°$, $T = 35°C$ ($\triangledown$), 25°C ($\circ$) and 20°C ($\diamond$) and $\phi_{tot} = 0.12$ (**a**) and 0.25 (**b**). The time-axes have been normalized with the free decay time $\tau_0 = (D_0 q^2)^{-1}$. Also shown are stretched exponential fits to the initial 20% of the decays (--) and the corresponding stretching exponents β at all T (**c, d**). The colored symbols in **c** & **d** correspond to the temperatures shown in **a** & **b**.

mutual $\beta H{-}\gamma B$ interactions are present in the protein solutions, we compared our experimental data to hypothetical short-time local diffusion coefficients, ignoring specific mutual interactions (open symbols in figure 5.3b), calculated as described in detail for $\alpha/\gamma B$ mixtures in Paper VI. We see that $\beta H{-}\gamma B$ interactions must be present, as the measured values of the local dynamics are significantly lower than the hypothetical ones.

6

Conclusion and Outlook

In chapter 4, a combination of DLS and NSE has allowed us to investigate the dynamic behavior of all three individual components of the eye lens on different length scales and we found that they become macroscopically arrested at $\phi_{\text{arr}}^{\alpha} = 0.58$, $\phi_{\text{arr}}^{\beta H} = 0.62$, $\phi_{\text{arr}}^{\gamma B} = 0.35$. Considering protein concentration instead of volume fraction, it becomes obvious, that all three proteins undergo dynamical slowing down on local length scales and become macroscopically arrested at physiologically relevant concentrations, as summarized in figure 6.1. This suggests that the gradual hardening of the eye lens which is at the basis of the development of presbyopia might be linked to an arrest transition of the concentrated protein mixture in the eye lens cells.

Using NSE, we were additionally able to show that critical slowing down, found in systems with short-range attractions, is a collective phenomenon not affecting the local motion of proteins, whereas dynamical arrest at large ϕ is a true arrest. We demonstrated, through a combination of experiments and computer simulations, that the cause of this arrest depends on the interaction potential of the proteins, as well as the anisotropy of these interactions. For pure hard spheres (α-crystallin), arrest is caused by caging by neigboring particles with the proteins still rattling in their nearest-neighbor cage, a state known as a repulsive glass. For particles with weak short-range attractions (βH-crystallin), the dynamics at
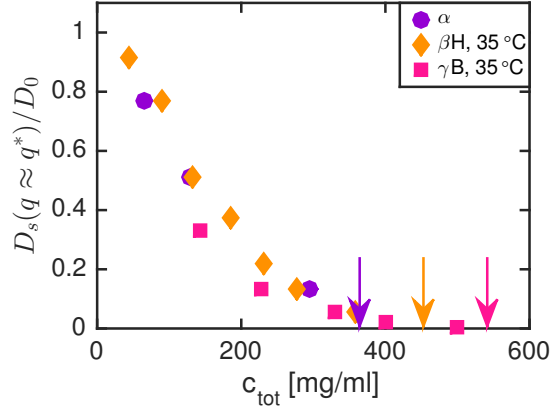
45

Figure 6.1: Short-time local dynamics of α-, βH- and γB-crystallin on length scales corresponding to the nearest-neighbor distance d^*. The arrows indicate the volume fractions where macroscopic arrest occurs.

intermediate ϕ are slowed down more than in the case of pure excluded volume interactions. At large volume fractions, however, the attractions push the arrest towards larger ϕ, due to the large polydispersity and possibly also as a result of the weak attraction. In the case of anisotropic patchy attractions (γB-crystallin), the patches on the protein surface induce temporary bonds between the proteins which lead to a dynamical arrest on all length scales at a volume fraction where caging by neighboring particles is still negligible.

Our hypothesis of the molecular origin of presbyopia was further corroborated by studies of binary mixtures of eye lens proteins ($\alpha/\gamma B$ and $\beta H/\gamma B$). In chapter 5, we showed that these mixtures also exhibit critical slowing down, affecting their collective dynamics and that they undergo dynamical slowing with increasing ϕ_{tot}. Additionally, we find that mutual attractions between unlike proteins influence the solution dynamics of these binary mixtures on short length scales, leading to smaller values of the short-time local diffusion coefficients than expected for solutions without specific mutual interactions. Figure 6.2 summarizes the dynamics of solutions of the pure proteins, together with those of binary $\alpha/\gamma B$ and $\beta H/\gamma B$ mixtures, on different length scales, as a function of total protein concentration. This representation shows that especially the collective dynamics are affected by the presence of α- or βH-crystallin in the solutions, speading them up considerably, compared to solutions of pure γB-crystallin at the same total concentrations. This effect is stronger for α-crystallin than for βH-crystallin.
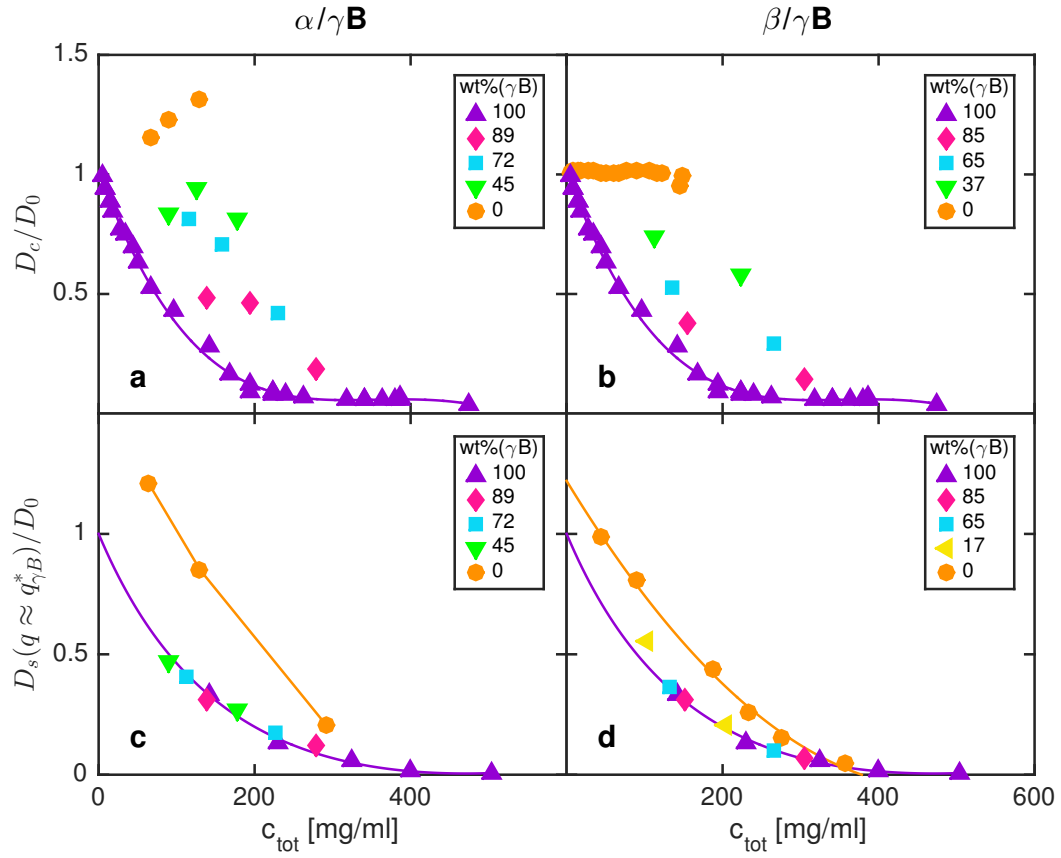
Figure 6.2: Normalized short-time collective (**a**, **b**) and local (**c**, **d**) diffusion coefficients of $\alpha/\gamma B$ (**a**, **c**) and of $\beta/\gamma B$ mixtures (**b**, **d**). **a**-**c**: 35°C, **d**: 25°C. The lines are guides to the eye.

Additionally, we found that βH-crystallin stabilizes solutions of γB-crystallin (i.e. moves T_c to lower values), compared to solutions of pure γB-crystallin at the same total protein concentration, as shown in figure 6.3b, thus preventing phase separation and increased light scattering. For $\alpha/\gamma B$-mixtures, the situation is more complex, as shown in figure 6.3a.
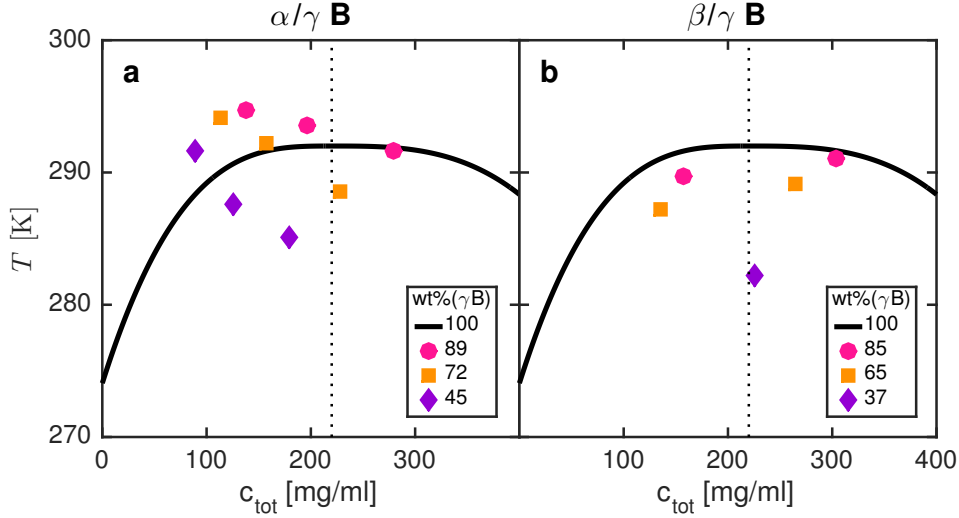

Figure 6.3: Binodals (or cloud temperatures) of $\alpha/\gamma B$ mixtures (**a**) and of $\beta/\gamma B$ mixtures (**b**) at varying protein content. The dotted line marks the critical concentration of γB-crystallin.

This shows that the actual relative protein composition of the eye lens fibre cells is a subtle balance between improving stability (lower risk of developing cataract) and ensuring liquid-like dynamics (lower risk of developing presbyopia), all the while keeping in mind that in order to be able to function as a lens, the eye lens has to be transparent and have a large refractive index. *In vivo*, transparency is mostly guaranteed by the even distribution of crystallins in the lens fibre cells. A large refractive index, on the other hand, is obtained with a high protein concentration in the lens [1]. Considering that α- and βH-crystallin have an open non-compact, multi-subunit structure [1, 2] and thus a large voluminosity, as discussed in the chapter 4, it is not possible to obtain the required high concentrations using large proportions of these proteins. γ_B-crystallin, on the other hand, has a monomeric compact structure, and conversely a low voluminosity, thus generating a larger refractive index then the other two proteins at the same concentration. From a refractive index point of view it is thus favorable to have large proportions of γB-crystallin. Our results however show that concentrated solutions of pure γB-crystallin are unstable and prone to phase separate and to macroscopically arrest at physiologically relevant

concentrations and that addition of α- and/or βH-crystallin to the solution improves solution stability and dynamics.

To arrive at a complete understanding of the eye lens, more detailed studies of binary mixtures and ultimately of ternary mixtures of all three individual components over a large range of total concentrations/volume fractions, combining different experimental methods and computer simulations, will be necessary. The results presented here are an important step on the way to this ultimate goal, as understanding the individual proteins and binary mixtures will help the interpretation of data obtained for more complex systems.

References

(1) Bloemendal, H.; de Jong, W.; Jaenicke, R.; Lubsen, N. H.; Slingsby, C.; Tardieu, A. *Prog. Biophys. Mol. Biol.* **2004**, *86*, 407–485.
(2) Vérétout, F.; Delaye, M.; Tardieu, A. *J. Mol. Biol.* **1989**, *205*, 713–728.